

**A New Resonance Calculation Method using Energy Expansion Based on a
Reduced Order Model**

Ryoichi Kondo^{1*}, Tomohiro Endo¹, Akio Yamamoto¹, Satoshi Takeda², Hiroki Koike³,
Kazuya Yamaji³, Daisuke Sato³

¹Nagoya University:Furo-cho, Chikusa-ku, Nagoya, Japan, 464-8603

²Osaka University:2-1 Yamadaoka, Suita-shi, Osaka, Japan, 565-0871

³Mitsubishi Heavy Industries, Ltd.:1-1-1 Wadasaki-Cho, Hyogo-ku, Kobe, Japan, 652-
8585

*) Corresponding author: r-kondo@fermi.energy.nagoya-u.ac.jp, Tel. +81-52-789-3775,
Fax. +81-51-789-3608

ABSTRACT

A Resonance calculation using energy Spectrum Expansion (RSE) method is newly proposed in this paper. In this method, ultra-fine group spectra appeared in a resonance calculation are expanded by orthogonal bases on energy, which are extracted from the ultra-fine group spectra obtained in homogeneous geometry with various background cross sections using singular value decomposition (SVD) and low-rank-approximation (LRA). Namely, this method is based on a concept of a reduced order model (ROM). Neutron transport equation for flux moments (expansion coefficients) similar to the conventional one is derived and is numerically solved. This method applied to two benchmark problems in which resonance interference effect and spatial self-shielding effect can appear. The results indicate that this method accurately predicts the reference effective cross sections and reaction rates obtained from direct ultra-fine group calculation in heterogeneous geometry.

KEYWORDS: Resonance calculation, effective cross section, ultra-fine group spectrum, reduced order model, singular value decomposition

I. INTRODUCTION

Resonance calculation is one of the most important and difficult parts in core analysis and can dominate prediction accuracy of core analysis. To treat steep and complicated variations of cross sections (resonances) accurately and efficiently, various approaches have been developed. The approaches are roughly classified into three categories: the equivalence theory [1], the ultra-fine group theory [2], and the subgroup theory [3]. Each of the approaches has advantages and disadvantages. The equivalence theory has been a historical approach and is still widely used in current core analyses owing to its efficiency. The equivalence theory adopts many assumptions and approximations thus its accuracy is inevitably limited [4]. For example, accurate consideration of resonance interference effect [5][6] among different nuclides or space-dependent resonance shielding effect in a generalized geometry is difficult. The ultra-fine group theory utilizes “first-principles” to calculate detailed energetic and spatial dependence of neutron spectra. In principle, this approach is very accurate but requires large computational resources, especially for large geometry. This approach is commonly used for single pin-cell calculations but its application to larger geometries, *e.g.*, single fuel assembly, is still prohibitive for production calculations. The last one, the subgroup theory, divides an energy group into subgroup considering magnitude of cross sections since shape of neutron spectrum is dominated by the magnitude of cross sections. The subgroup theory offers an efficient pathway to treat resonance effect in a generalized geometry thus is currently used in various up-to-date core analysis codes that explicitly handle heterogeneous core geometry. Potential drawback of the subgroup theory is a consideration of resonance interference effect among different nuclides and regions, including treatment of non-uniform temperature distribution [7]. Various improvements have been proposed to overcome these issues.

This study considered an alternative approach to resonance treatment. In this approach, energy dependence of neutron spectrum (angular flux) in an energy range (within a multi-group) was expanded by orthogonal functions (orthogonal bases) on energy. Function expansion of angular or scalar flux was traditionally used, *e.g.*, use of spherical harmonics functions for angular dependence, use of polynomials for spatial dependence in advanced nodal method. Previous works had studied the application of function expansion for energy dependence of neutron spectrum. Rahnema and Zhu et al. had applied Legendre polynomials to represent a fine structure of neutron flux in a multi-

group [8][9]. Their objective is an improvement of the accuracy in conventional multi-group calculations. Tellier, Yang, and Rooijen et al. had utilized Wavelet functions to describe energy dependence of neutron flux at resonance energy regions [10][11][12]. However, Rooijen reported that the number of expansion functions to describe complicated resonances becomes large thus the efficiency of this approach is limited [12].

This study adopted energy function expansion as well as the previous studies, but different expansion functions were used that are based on numerically calculated ultra-fine group spectra. Fundamental insights behind the present study are described as follows.

Shape of ultra-fine group neutron spectrum is energetically very complicated, it mainly depends on material composition, temperature, and spatial position in a resonance material. Equivalence theory shows that variation of an ultra-fine group spectrum can be approximately described by rational approximation and background cross section that represents self-shielding condition [13][14][15]. This means that, though the energy dependence of a neutron spectrum is very complicated in the resonance energy range, it can be represented by a relatively simple model, *i.e.*, reduced order model (ROM) [16].

In this study, energy expansion functions were numerically generated by ultra-fine group calculations in a simple (homogeneous) geometry considering various background cross sections. Singular value decomposition (SVD) and low-rank-approximation (LRA) [17][18] were used for ultra-fine group spectra to generate orthogonal bases for energy expansion.

Theoretical consideration of this method, Resonance calculation using energy Spectrum Expansion (RSE) method, is described in Sec. II. Numerical results and discussion are shown in Sec. III. Finally, concluding remarks are summarized in Sec. IV.

II. THEORY

II.A. Overview

In this subsection, the overview of the RSE method is described. In the present method, pointwise neutron spectra in an energy range are expanded by orthogonal bases on energy. Considering the expansion by the orthogonal basis, the transport equation for the flux moments (expansion coefficients) is derived. The transport equation for the flux moments is similar to the conventional one, thus it can be numerically solved. The RSE method can be applied to any type of transport calculation method. In the present study,

the method is implemented with the method of characteristics (MOC) since MOC is commonly used for lattice physics calculation. Derivation of the transport equation for flux moments is described in Sec. II.B.

The orthogonal bases are generated by ultra-fine group spectra obtained in homogeneous geometry with various background cross sections. In this process, orthogonal bases are efficiently extracted using the SVD and the LRA. The choice of the orthogonal basis is crucial because the computational efficiency of the present method depends on how well an orthogonal basis captures the characteristics of various spectra in a calculation system. Note that ultra-fine group calculations are necessary in the RSE method, but their computational cost is trivial since they are calculated in homogeneous geometry. Detail descriptions of the generation method of orthogonal bases are provided in Sec. II.C.

Treatment of scattering (slowing down) source is another key point of the present method. There are two choices for the treatment of scattering source. The first one is the utilization of scattering matrix for flux moments. The scattering matrix for flux moments tends to become large because transfer between different expansion modes should be considered in addition to the conventional group to group transfer. In order to address this issue, the second approach is adopted in the present study, *i.e.*, the scattering source is directly calculated by solving the slowing down equation for a homogeneous medium. Calculation flow for flux moment including treatment of scattering source is described in Sec. II.D.

In Sec. II.E, some implementation details of the RSE method with MOC are described. Finally, the calculation procedures of the present method are provided in Sec. II.F.

II.B. Derivation of Transport Equation with Energy Expansion Bases

In this subsection, a transport equation with energy expansion bases is derived from the conventional one. The transport equation for a fixed source problem is:

$$\begin{aligned} & \boldsymbol{\Omega} \cdot \nabla \Psi(\mathbf{r}, \boldsymbol{\Omega}, E) + \Sigma_t(\mathbf{r}, E) \Psi(\mathbf{r}, \boldsymbol{\Omega}, E) \\ &= \frac{1}{4\pi} \int_0^\infty dE' \int_{4\pi} \Sigma_s(\mathbf{r}, E' \rightarrow E, \boldsymbol{\Omega}' \rightarrow \boldsymbol{\Omega}) \Psi(\mathbf{r}, \boldsymbol{\Omega}', E') d\boldsymbol{\Omega}' + q(\mathbf{r}, \boldsymbol{\Omega}, E), \end{aligned} \quad (1)$$

where \mathbf{r} : position vector, $\boldsymbol{\Omega}$: direction vector, E : energy, $\Psi(\mathbf{r}, \boldsymbol{\Omega}, E)$: angular flux, $\Sigma_t(\mathbf{r}, E)$: macroscopic total cross section, $\Sigma_s(\mathbf{r}, E' \rightarrow E, \boldsymbol{\Omega}' \rightarrow \boldsymbol{\Omega})$: macroscopic scattering

cross section, $q(\mathbf{r}, \boldsymbol{\Omega}, E)$: fixed source. Note that the eigenvalue calculation is not necessary and the fixed source treatment is sufficient in the resonance calculation.

Isotropic scattering and isotropic neutron sources are assumed:

$$\begin{aligned}
& \boldsymbol{\Omega} \cdot \nabla \Psi(\mathbf{r}, \boldsymbol{\Omega}, E) + \Sigma_t(\mathbf{r}, E) \Psi(\mathbf{r}, \boldsymbol{\Omega}, E) \\
&= \frac{1}{4\pi} \int_0^\infty \Sigma_s(\mathbf{r}, E' \rightarrow E) \int_{4\pi} \Psi(\mathbf{r}, \boldsymbol{\Omega}', E') d\boldsymbol{\Omega}' dE' \\
&+ \frac{1}{4\pi} Q(\mathbf{r}, E) \\
&= \frac{1}{4\pi} \int_0^\infty \Sigma_s(\mathbf{r}, E' \rightarrow E) \phi(\mathbf{r}, E') dE' + \frac{1}{4\pi} Q(\mathbf{r}, E),
\end{aligned} \tag{2}$$

where

$$\begin{aligned}
\phi(\mathbf{r}, E') &= \int_{4\pi} \Psi(\mathbf{r}, \boldsymbol{\Omega}', E') d\boldsymbol{\Omega}', \\
Q(\mathbf{r}, E) &= \int_{4\pi} q(\mathbf{r}, \boldsymbol{\Omega}, E) d\boldsymbol{\Omega}.
\end{aligned} \tag{3}$$

The assumption of isotropic source is justified in resonance calculation since anisotropic scattering has a small impact on resonance treatment [19]. By considering an energy range (energy range for multi-group g or g' , $1 \leq g \leq G$, $1 \leq g' \leq G$), Eq.(2) can be written as:

$$\begin{aligned}
& \boldsymbol{\Omega} \cdot \nabla \Psi(\mathbf{r}, \boldsymbol{\Omega}, E_g) + \Sigma_t(\mathbf{r}, E_g) \Psi(\mathbf{r}, \boldsymbol{\Omega}, E_g) \\
&= \sum_{g'=1}^G \frac{1}{4\pi} \int_{\Delta E_{g'}} \Sigma_s(\mathbf{r}, E_{g'} \rightarrow E_g) \phi(\mathbf{r}, E_{g'}) dE_{g'} \\
&+ \frac{1}{4\pi} Q(\mathbf{r}, E_g).
\end{aligned} \tag{4}$$

where E_g is the energy range for g -th energy group.

Angular flux, scalar flux, and external source are expanded by the orthogonal bases on energy:

$$\Psi(\mathbf{r}, \boldsymbol{\Omega}, E_g) = \sum_{i=1}^N f_{i,g}(E_g) \Psi_{i,g}(\mathbf{r}, \boldsymbol{\Omega}), \tag{5}$$

$$\begin{aligned}
\phi(\mathbf{r}, E_g) &= \int_{4\pi} \Psi(\mathbf{r}, \boldsymbol{\Omega}, E_g) d\boldsymbol{\Omega} = \int_{4\pi} \sum_{i=1}^N f_{i,g}(E_g) \Psi_{i,g}(\mathbf{r}, \boldsymbol{\Omega}) d\boldsymbol{\Omega} \\
&= \sum_{i=1}^N f_{i,g}(E_g) \phi_{i,g}(\mathbf{r}),
\end{aligned} \tag{6}$$

$$Q(\mathbf{r}, E_g) = \sum_{i=1}^N f_{i,g}(E_g) Q_{i,g}(\mathbf{r}), \quad (7)$$

where i : order of expansion, N : maximum order of expansion, $f_{i,g}(E_g)$: orthogonal basis, $\Psi_{i,g}(\mathbf{r}, \boldsymbol{\Omega})$: expansion coefficient for angular flux, $Q_{i,g}(\mathbf{r})$: expansion coefficient for neutron source, and $\phi_{i,g}(\mathbf{r})$: expansion coefficient for scalar flux defined by Eq. (8),

$$\phi_{i,g}(\mathbf{r}) = \int_{4\pi} \Psi_{i,g}(\mathbf{r}, \boldsymbol{\Omega}) d\boldsymbol{\Omega}. \quad (8)$$

The orthogonal property of the bases is:

$$\int_{\Delta E_g} f_{i,g}(E_g) f_{j,g}(E_g) dE_g = \delta_{ij}, \quad (9)$$

where δ_{ij} is the Kronecker delta. Thus, the coefficients are obtained by Eq. (10).

$$\begin{aligned} \Psi_{i,g}(\mathbf{r}, \boldsymbol{\Omega}) &= \int_{\Delta E_g} f_{i,g}(E_g) \Psi(\mathbf{r}, \boldsymbol{\Omega}, E_g) dE_g, \\ \phi_{i,g}(\mathbf{r}) &= \int_{\Delta E_g} f_{i,g}(E_g) \phi(\mathbf{r}, E_g) dE_g, \\ Q_{i,g}(\mathbf{r}) &= \int_{\Delta E_g} f_{i,g}(E_g) Q(\mathbf{r}, E_g) dE_g, \end{aligned} \quad (10)$$

Equation (11) is obtained by substituting Eqs. (5), (6), and (7) into Eq. (4).

$$\begin{aligned} \boldsymbol{\Omega} \cdot \nabla \sum_{i=1}^N f_{i,g}(E_g) \Psi_{i,g}(\mathbf{r}, \boldsymbol{\Omega}) + \Sigma_t(\mathbf{r}, E_g) \sum_{i=1}^N f_{i,g}(E_g) \Psi_{i,g}(\mathbf{r}, \boldsymbol{\Omega}) \\ = \sum_{g'=1}^G \frac{1}{4\pi} \int_{\Delta E_{g'}} \Sigma_s(\mathbf{r}, E_{g'} \rightarrow E_g) \sum_{j=1}^N f_{j,g'}(E_{g'}) \phi_{j,g'}(\mathbf{r}) dE_{g'} \\ + \frac{1}{4\pi} \sum_{i=1}^N f_{i,g}(E_g) Q_{i,g}(\mathbf{r}). \end{aligned} \quad (11)$$

Equation (12) is obtained by multiplying $f_{n,g}(E_g)$ to the both sides of Eq.(11), performing energy integration for ΔE_g , and applying the orthogonal property of Eq. (9):

$$\begin{aligned} \boldsymbol{\Omega} \cdot \nabla \Psi_{n,g}(\mathbf{r}, \boldsymbol{\Omega}) + \sum_{i=1}^N \Sigma_{t,g,n,i}(\mathbf{r}) \Psi_{i,g}(\mathbf{r}, \boldsymbol{\Omega}) \\ = \frac{1}{4\pi} \sum_{g'=1}^G \sum_{j=1}^N \Sigma_{s,jg' \rightarrow ng}(\mathbf{r}) \phi_{j,g'}(\mathbf{r}) + \frac{1}{4\pi} Q_{n,g}(\mathbf{r}), \end{aligned} \quad (12)$$

where

$$\Sigma_{t,g,n,i}(\mathbf{r}) = \int_{\Delta E_g} f_{n,g}(E_g) \Sigma_t(\mathbf{r}, E_g) f_{i,g}(E_g) dE_g, \quad (13)$$

$$\Sigma_{s,jg' \rightarrow ng}(\mathbf{r}) = \int_{\Delta E_g} \int_{\Delta E_{g'}} f_{n,g}(E_g) \Sigma_s(\mathbf{r}, E_{g'} \rightarrow E_g) f_{j,g'}(E_{g'}) dE_{g'} dE_g.$$

Equation (12) is similar to the conventional multi-group transport equation but the collision term (the second term of the left-hand side) is replaced by the summation on N terms. It means that Eq. (12) is the first order simultaneous differential equations in which N equations are coupled for a group g . It should be noted that scattering matrix becomes more complicated than that of the conventional one since the transfer from mode j to n is included in addition to energy transfer from g' to g .

II.C. Generation of Orthogonal Bases

The choice of the orthogonal bases is a key point of the present method. In principle, an ultra-fine group calculation is carried out for an entire calculation geometry, *e.g.*, a fuel assembly or a reactor core, then the orthogonal bases are generated using the results. Since all ultra-fine group spectra appeared in the calculation are contained in such calculation result, ideal orthogonal bases can be constructed. On the other hand, the essential issue of this approach is practicality. An ultra-fine group calculation for a reactor core (even for a fuel assembly) takes prohibitive computation time. Furthermore, if the ultra-fine group results exist, one can use them to generate accurate effective cross sections.

To generate appropriate orthogonal bases within the practical computation time, the following approach can be considered:

- (a) Perform ultra-fine group calculations in a single pin-cell (or 3×3 pin-cells) for typical state points, fuel compositions, and temperatures.
- (b) Perform ultra-fine group calculations in a homogeneous geometry for typical fuel compositions, temperatures, and background cross sections.
- (c) Perform ultra-fine group calculations in a homogeneous geometry for typical resonance nuclides, temperatures, and background cross sections.

The approach (a) incorporates the current practice that the ultra-fine group calculation is carried out in a small geometry, typically in a pin-cell. On the other hand, the approach (b) or (c) implicitly utilizes the equivalence theory that the ultra-fine group spectrum can be approximately reproduced with appropriate background cross sections. The approach

(c) is the current practice to generate multi-group microscopic cross section library for a lattice physics code. The advantage of the approach (c) is simplicity but the resonance interference effect among different nuclides cannot be taken into account. On the contrary, the approach (b) can explicitly consider the resonance interference effect while suppressing computation time. In the present study, the approach (b) is used.

Once various ultra-fine group spectra are obtained, orthogonal bases to approximately reproduce the ultra-fine group spectra are extracted as follows. As shown in Eq. (5), the orthogonal bases are multi-group dependent, *i.e.*, different bases are used for different multi-group. In a multi-group, the identical orthogonal basis should be used for whole calculation geometry. Namely, in Eq. (10), the same $f_{i,g}(E_g)$ used for different regions in a calculation geometry. Therefore, the ultra-fine group spectra generated by the method (a), (b) and/or (c) should cover the variation that appeared throughout a calculation geometry.

The orthogonal bases should reproduce the ultra-fine group spectra as accurately as possible. To achieve this goal, the SVD and the LRA are used [17][18]. This approach is one of the concepts of ROM [16]. The SVD decomposes a matrix to a diagonal matrix and orthogonal matrixes [20]. Let us consider that m ultra-fine group spectra and each spectrum consists of t ultra-fine energy groups in a specific energy range (within a multi-group). These ultra-fine group spectra can be arranged as a matrix \mathbf{A} , whose size is $m \times t$:

$$\mathbf{A} = \begin{pmatrix} \phi_1(E_1) & \cdots & \phi_1(E_t) \\ \vdots & \ddots & \vdots \\ \phi_m(E_1) & \cdots & \phi_m(E_t) \end{pmatrix}. \quad (14)$$

Using $\mathbf{U} = (\vec{u}_1, \vec{u}_2, \dots, \vec{u}_m)$ and $\mathbf{V} = (\vec{v}_1, \vec{v}_2, \dots, \vec{v}_t)$, the matrix \mathbf{A} is transformed into a $m \times t$ diagonal matrix $\mathbf{\Sigma}$:

$$\mathbf{U}^T \mathbf{A} \mathbf{V} = \mathbf{\Sigma}, \quad (15)$$

where

$$\mathbf{\Sigma} = \begin{pmatrix} \sigma_1 & 0 & \cdots & \cdots & \cdots & 0 \\ 0 & \sigma_2 & 0 & \ddots & \ddots & \vdots \\ \vdots & \ddots & \ddots & 0 & \ddots & \vdots \\ 0 & \cdots & 0 & \sigma_m & \cdots & 0 \end{pmatrix}. \quad (16)$$

The diagonal components are the singular values having the following property; $\sigma_1 > \sigma_2 > \cdots > \sigma_i \geq 0$ ($1 \leq i \leq m$). The number of m corresponds to the rank of matrix \mathbf{A} . Since the \mathbf{U} and \mathbf{V} are unitary matrixes, Eq. (15) can be transformed as:

$$\begin{aligned}
\mathbf{U}^T \mathbf{U} \mathbf{A} \mathbf{V}^T \mathbf{V} &= \mathbf{U} \boldsymbol{\Sigma}^T \mathbf{V}, \\
\mathbf{U} \mathbf{U}^{-1} \mathbf{A} \mathbf{V} \mathbf{V}^{-1} &= \mathbf{U} \boldsymbol{\Sigma}^T \mathbf{V}, \\
\mathbf{A} &= \mathbf{U} \boldsymbol{\Sigma}^T \mathbf{V},
\end{aligned} \tag{17}$$

where \mathbf{U} is the left singular vectors, $\boldsymbol{\Sigma}$ is the singular values, and \mathbf{V} is the right singular vectors. The cumulative contribution ratio of the singular vectors is calculated by:

$$(\text{The cumulative contribution ratio of the } 1^{\text{st}} - k^{\text{th}} \text{ vectors}) = \frac{\sum_{i=1}^k \sigma_i^2}{\sum_{i=1}^m \sigma_i^2}. \tag{18}$$

For example, if the cumulative contribution ratio up to the k -th vector is 0.99, the $1^{\text{st}} - k^{\text{th}}$ vectors can represent 99% of the variation of elements (in precise, the variance of elements) in matrix \mathbf{A} , which means these vectors almost captures the behavior of the matrix \mathbf{A} . This is a basic concept of LRA, *i.e.*, even if the small singular values are truncated, the matrix \mathbf{A} can be accurately reconstructed by the rest of singular vectors and singular values.

The matrix \mathbf{A} , whose rank is m ($m < t$), is written as:

$$\mathbf{A} = (\vec{u}_1, \vec{u}_2, \dots, \vec{u}_m) \begin{pmatrix} \sigma_1 & 0 & \dots & \dots & \dots & 0 \\ 0 & \sigma_2 & 0 & \ddots & \ddots & \vdots \\ \vdots & \ddots & \ddots & 0 & \ddots & \vdots \\ 0 & \dots & 0 & \sigma_m & \dots & 0 \end{pmatrix}^T (\vec{v}_1, \vec{v}_2, \dots, \vec{v}_t). \tag{19}$$

Let us assume that the major behavior of matrix \mathbf{A} can be reproduced by the first k singular values ($k \leq m$). Then the matrix \mathbf{A} can be approximated as Eq. (20). The singular value is represented by a square matrix of $k \times k$.

$$\mathbf{A} \approx \mathbf{A}' = (\vec{u}_1, \vec{u}_2, \dots, \vec{u}_k) \begin{pmatrix} \sigma_1 & 0 & \dots & 0 \\ 0 & \sigma_2 & \ddots & \vdots \\ \vdots & \ddots & \ddots & 0 \\ 0 & \dots & 0 & \sigma_k \end{pmatrix}^T (\vec{v}_1, \vec{v}_2, \dots, \vec{v}_k). \tag{20}$$

The approximated matrix \mathbf{A}' can be reconstructed by the truncated orthogonal bases

$${}^T (\vec{v}_1, \vec{v}_2, \dots, \vec{v}_k) \text{ and expansion coefficients } (\vec{u}_1, \vec{u}_2, \dots, \vec{u}_k) \begin{pmatrix} \sigma_1 & 0 & \dots & 0 \\ 0 & \sigma_2 & \ddots & \vdots \\ \vdots & \ddots & \ddots & 0 \\ 0 & \dots & 0 & \sigma_k \end{pmatrix}.$$

Therefore, part of the matrix \mathbf{V} obtained by the SVD can be used for the orthogonal basis for the ultra-fine group spectra.

Through the SVD, we can choose the dominant expansion bases to reproduce the ultra-fine group spectra. The efficiency of the present orthogonal bases depends on the behavior of singular values. If the singular values decay rapidly as the order increases, the small number of orthogonal bases efficiently reproduces the ultra-fine group spectra.

II.D. Treatment of Scattering Source

As shown in Eq. (13), the moments of scattering cross sections ($\Sigma_{s,jg' \rightarrow ng}(\mathbf{r})$) are necessary to solve the transport equation Eq. (12). However, they can become large because the “mode-to-mode” transfer is necessary in addition to the conventional energy “group-to-group” transfer. For example, let us consider self-scattering (in-group scattering) in an energy group in a region. In the conventional transport equation, a scalar value of the self-scattering cross section is sufficient. However, in Eq. (13), the moments of scattering cross section from mode i to j is necessary for self-scattering. In the present study, the right term of Eq. (12) is solved using the slowing down equation [4] to reduce the size of the moments of scattering cross sections. Note that the slowing down calculation is carried out in each region.

Equation (12) is re-written as follows:

$$\boldsymbol{\Omega} \cdot \nabla \Psi_{n,g}(\mathbf{r}, \boldsymbol{\Omega}) + \sum_{i=1}^N \Sigma_{t,g,n,i}(\mathbf{r}) \Psi_{i,g}(\mathbf{r}, \boldsymbol{\Omega}) = Q_{n,g}(\mathbf{r}), \quad (21)$$

where

$$Q_{n,g}(\mathbf{r}) = \int_{\Delta E_g} f_{n,g}(E_g) Q(\mathbf{r}, E_g) dE_g, \quad (22)$$

$$Q(\mathbf{r}, E_g) = Q_{slid}(\mathbf{r}, E_g) + Q_{fixed}(\mathbf{r}, E_g),$$

where $Q_{fixed}(\mathbf{r}, E_g)$: fixed source, $Q_{slid}(\mathbf{r}, E_g)$: slowing down source. The fixed source is typically given by the fission source in a fuel region. Since the spatial distribution of the fixed source does not significantly impact on the resonance treatment, spatially flat fission source can be used. Slowing down source is calculated by the slowing down equation Eq. (23) by applying the isotropic and elastic scattering in the center-of-mass system for scattering:

$$Q_{slid}(\mathbf{r}, E_g) = \sum_k \int_{E_g}^{E_g/\alpha_k} N_k \sigma_{s,k}(\mathbf{r}, E) \frac{\phi(\mathbf{r}, E)}{(1 - \alpha_k)E} dE, \quad (23)$$

where $\sigma_{s,k}(\mathbf{r}, E)$: microscopic elastic scattering cross section for nuclide k , $\alpha_k = \left(\frac{A_k-1}{A_k+1}\right)^2$: maximum energy loss ratio for nuclide k , A_k : relative atomic weight of nuclide k to the neutron. Note that the angle of the scattering is defined in the center-of-mass system but neutron energy is described in the laboratory system. Equation (23) should be solved in all regions. The scalar flux: $\phi(\mathbf{r}, E)$ and thus the slowing down source: $Q_{slid}(\mathbf{r}, E_g)$ are obtained iteratively as described in Sec. II.F. It should be noted that the

numerical solution of Eq. (23) is established since it has been widely used for ultra-fine spectrum calculations and it can be carried out with small computation time when the recurrence relation among ultra-fine group energy is used [4].

II.E. Implementation with MOC

In the present study, the RSE method is implemented with MOC (in two-dimensional geometry) which is a popular transport method in lattice physics calculations. By applying the flat flux and constant macroscopic approximations in a region, and by discretizing the neutron flight direction, Eq. (21) can be written as:

$$\frac{d}{ds}\Psi_{n,g,r,m}(s) + \sum_{i=1}^N \Sigma_{t,g,n,i,r} \Psi_{i,g,r,m}(s) = Q_{n,g,r}, \quad (24)$$

where s is the coordinate along neutron flight direction, $\Psi_{n,g,r,m}$ and $Q_{n,g,r}$ are angular flux and neutron source of n -th moment, energy group g , region r , neutron flight direction m , respectively, $\Sigma_{t,g,n,i,r}$ is average total cross section moment in region r . They are defined by:

$$\begin{aligned} \Psi_{n,g,r,m}(s) &= \Psi_{n,g}(\mathbf{r}, \boldsymbol{\Omega}_m), \\ Q_{n,g,r} &= \frac{1}{4\pi} \frac{\int_{\mathbf{r} \in r} Q_{n,g}(\mathbf{r}) d\mathbf{r}}{\int_{\mathbf{r} \in r} d\mathbf{r}}, \\ \Sigma_{t,g,n,i,r} &= \frac{\int_{\mathbf{r} \in r} \Sigma_{t,g,n,i}(\mathbf{r}) d\mathbf{r}}{\int_{\mathbf{r} \in r} d\mathbf{r}}. \end{aligned} \quad (25)$$

Equation (24) is similar to the conventional MOC transport equation, but the collision term contains contributions from multiple angular flux moments. Equation (24) is the simultaneous differential equation thus can be solved by several numerical methods. One of the simplest approaches is the utilization of the Jacobi or the Gauss-Seidel iteration in which Eq. (24) is treated by:

$$\frac{d}{ds}\Psi_{n,g,r,m}(s) + \Sigma_{t,g,n,n,r} \Psi_{n,g,r,m}(s) = Q_{n,g,r} - \sum_{i \neq n} \Sigma_{t,g,n,i,r} \Psi_{i,g,r,m}(s). \quad (26)$$

Equation (26) has an identical form with the conventional MOC transport equation except for the additional terms in the right hand side thus can be easily solved by existing MOC codes. Note that the flat angular flux assumption can be used for $\Psi_{i,g,r,m}(s)$ in the right hand side of Eq. (26). However, unfortunately, our preliminary study reveals that the total cross section moments may not be diagonal dominant (*i.e.*, $\Sigma_{t,g,n,i,r} > \Sigma_{t,g,n,n,r}$, $i \neq n$)

thus an iterative solution using the Jacobi or the Gauss-Seidel method could not be used. Instead, in the present study, Eq. (24) is written as the vector-matrix form as:

$$\begin{aligned} \frac{d}{ds} \vec{\Psi}_{g,r,m}(s) + \Sigma_{t,g,r} \vec{\Psi}_{g,r,m}(s) &= \vec{Q}_{g,r}, \\ \vec{\Psi}_{g,r,m}(s) &= {}^T(\Psi_{1,g,r,m}(s) \quad \Psi_{2,g,r,m}(s) \quad \dots \quad \Psi_{N,g,r,m}(s)), \\ \Sigma_{t,g,r} &= \begin{pmatrix} \Sigma_{t,g,1,1,r} & \Sigma_{t,g,1,2,r} & \dots & \Sigma_{t,g,1,N,r} \\ \Sigma_{t,g,2,1,r} & \Sigma_{t,g,2,2,r} & \ddots & \vdots \\ \vdots & \ddots & \ddots & \vdots \\ \Sigma_{t,g,N,1,r} & \dots & \dots & \Sigma_{t,g,N,N,r} \end{pmatrix}, \\ \vec{Q}_{g,r} &= {}^T(Q_{1,g,r} \quad Q_{2,g,r} \quad \dots \quad Q_{N,g,r}). \end{aligned} \quad (27)$$

The solution of Eq. (27) is given by:

$$\vec{\Psi}_{g,r,m}(s) = e^{-\Sigma_{t,g,r}s} \vec{\Psi}_{g,r,m}(0) + (\mathbf{I} - e^{-\Sigma_{t,g,r}s}) \Sigma_{t,g,r}^{-1} \vec{Q}_{g,r}, \quad (28)$$

where $e^{-\Sigma_{t,g,r}s}$ and \mathbf{I} are the matrix exponential and the identity matrix, respectively. The average angular flux moments of g -th group, m -th direction, in r -th region $\vec{\Psi}_{g,r,m}$ is given by:

$$\vec{\Psi}_{g,r,m} = (\Sigma_{t,g,r} S)^{-1} (\vec{\Psi}_{g,r,m}(0) - \vec{\Psi}_{g,r,m}(S) + \vec{Q}_{g,r} S), \quad (29)$$

where S is the segment length of a region considering polar direction. In the present study, Eqs. (28) and (29) are numerically solved by Eigen [20].

Once the average angular flux moment in region r ($\vec{\Psi}_{g,r,m}$) is obtained, the scalar flux moment in region r is obtained by:

$$\begin{aligned} \vec{\phi}_{g,r} &= \sum_m \omega_m \vec{\Psi}_{g,r,m}, \\ \vec{\phi}_{g,r} &= {}^T(\phi_{1,g,r} \quad \phi_{2,g,r} \quad \dots \quad \phi_{N,g,r}), \end{aligned} \quad (30)$$

where $\vec{\phi}_{g,r}$ is the scalar flux moment in region r , ω_m is the weight for solid angle integration satisfying $\sum_m \omega_m = 4\pi$. Using the scalar flux moment in region r , ultra-fine group scalar flux in region r is obtained by Eq. (6).

II.F. Calculation Procedure of the RSE method

Calculation procedures of the RSE method are described based on the theory described in the previous subsections. The calculation flow to obtain effective cross sections is shown in Fig. 1.

Calculation procedures are as follows:

- (1) Generate ultra-fine group spectra using ultra-fine group slowing down calculations in homogeneous geometry for typical fuel compositions, temperatures, and background cross sections.
- (2) Generate the orthogonal bases $f_{n,g}(E_g)$ using SVD for ultra-fine group spectra obtained from step (1).
- (3) Prepare total cross section moment $\Sigma_{t,g,n,i,r}$ using Eq. (13). Note that constant cross section approximation is used.
- (4) Generate ray trace information for MOC.
- (5) Initialize i -th scalar flux moments $\phi_{i,g,r}$ in group g , region r . In the present study, spatially and energetically constant scalar flux distribution within a multi-group is assumed as the initial guess and it is expanded by the orthogonal basis to obtain initial scalar flux moments.
- (6) Initialize angular flux moments at boundaries assuming isotropic angular flux distribution, *i.e.*, $\Psi(\mathbf{r}, \mathbf{\Omega}_m, E_g) = \phi(\mathbf{r}, E_g)/4\pi$. Note that energetically constant angular flux distribution within a multi-group is assumed at the boundary and is expanded by the orthogonal basis.
- (7) Initialize source $Q_r(E_g)$ for group g , region r . The initial value of the slowing down source is set to be zero.
- (8) Calculate moments of source $Q_{n,g,r}$ by Eq. (22).
- (9) Perform transport sweep using Eq. (21) and estimate scalar flux moments $\phi_{n,g,r}$ in each region by solid angle integration of angular flux moment $\Psi_{n,g,r,m}$. This procedure is similar to that in the conventional MOC, *i.e.*, estimate scalar flux by solid angle integration of angular flux.
- (10) Reconstruct ultra-fine group spectra $\phi_r(E_g)$ by Eqs. (3) and (5).
- (11) Calculate slowing down source $Q_{sld,r}(E_g)$ in each region by Eq. (23).
- (12) Check the convergence of flux moments by Eq. (31):

$$\varepsilon_j = \left| \left(\left(\sum_n \phi_{n,g,r} \right)^{(j-1)} - \left(\sum_n \phi_{n,g,r} \right)^{(j)} \right) / \left(\sum_n \phi_{n,g,r} \right)^{(j)} \right|, \quad (31)$$

where ε_j is the relative residual of scalar flux moment at j -th iteration. It should be noted that the summation of scalar flux moments is used to check convergence in the present study since each flux moment can take a very small value and convergence check for small values is inefficient.

- (13) Update slowing down source if flux moments by Eq. (23) are not converged.
- (14) Repeat steps from (7) to (13) and calculate flux moments for all energy group.
- (15) Reconstruct ultra-fine group spectra $\phi_r(E_g)$ and calculate the effective cross section and the reaction rate by Eqs. (32) and (33), respectively.

$$\sigma_{x,g,r,eff}^k = \frac{\int_{\Delta E_g} \sigma_{x,r}^k(E) \phi_r(E) dE}{\int_{\Delta E_g} \phi_r(E) dE}, \quad (32)$$

where $\sigma_{x,g,r,eff}^k$ is the effective microscopic cross section of type x , energy group g , nuclide k , and region r , and $\sigma_{x,r}^k(E)$ is the microscopic cross section of type x , nuclide k , and region r .

$$R_{x,g,r}^k = \int_{\Delta E_g} N_r^k \sigma_{x,r}^k(E) \phi_r(E) dE, \quad (33)$$

where $R_{x,g,r}^k$ is the reaction rate and N_r^k is the number density.

III. CALCULATIONS

In section III, accuracy of RSE method was shown through analyses of benchmark problems. Three typical situations were considered that are important for resonance treatment. The first one was multi-cell geometry consist of UO₂ and MOX fuels in a typical light water reactor. The second one was a pin-cell geometry in which fuel pellet is annularly subdivided and temperature distribution inside a fuel pellet is considered. The last one was a unit assembly geometry. Accurate resonance treatment of these problems was difficult with conventional equivalent and sub-group methods due to resonance interference effect among regions. For reference calculation, direct ultra-fine group (UFG) calculation in the heterogeneous geometry using MOC was used.

III.A. Multi-cell Geometry

III.A.1. Calculation Conditions

Specifications of multi-cell geometries and unit pin-cell geometry used in the present study were shown in Fig. 2 and Table I, respectively. No gap between pellet and cladding was considered for simplicity. The numbers in Fig. 2-(a) were the identification to distinguish the same type of fuel. Since UO₂ and MOX fuel cells were adjacent in Fig. 2-(b), resonance interference effect between two fuel cells was observed. In order to confirm resonance interference effect in Fig. 2-(b), geometry of Fig. 2-(c) was also

considered. Composition of each material was shown in Table II. Temperature of all material was 600 K. Reflective boundary condition was assumed for all cases.

For pointwise cross sections used in the present method, ACE formatted cross sections, which were generated by FRENDY code [21] using JENDL-4.0 [22], were used. The generated ACE cross sections were also used for ultra-fine group (UFG) reference calculations by MOC. GENESIS code [23] was used as MOC transport solver for ultra-fine group calculation in a two-dimensional geometry. Calculation condition for the GENESIS code was shown in Table III. For convergence criterion of flux, scalar flux was used for reference UFG calculation and moment of scalar flux (Eq. (31)) was used for RSE calculation. Energy group structure for ultra-fine group calculation was shown in Table IV [25]. For multi-group structure, XMAS 172 group structure was adopted [4]. Orthogonal basis was independently generated in each of the 172 groups. It should be noted that though the resolved resonance usually appeared at intermediate energy range, RSE method was applied to all energy groups from fast to thermal energy range. For slowing down calculation, the only contribution from elastic scattering assuming isotropic scattering in the center-of-mass system was considered throughout the present study. Namely, only elastic scattering was considered in ultra-fine group spectrum calculations for construction of orthogonal basis, RSE calculation, and reference UFG calculation by MOC.

The number of ultra-fine group spectra used in Step (1)–(2) of calculation flow in Sec. II.F was 32, which came from the numbers of background cross sections for UO_2 and MOX (11 points for each material, totally 22 points), cladding (9 points) and H_2O (1 point) as shown in Table V. A maximum number of the orthogonal bases was given by the size of matrix \mathbf{A} shown in Eq. (14), *i.e.*, smaller size of rows or columns. Therefore, the maximum number of orthogonal bases was given by the smaller number of ultra-fine groups within a multi-group (columns of the matrix \mathbf{A}) or background cross sections (rows of the matrix \mathbf{A} , 32). Since the minimum number of ultra-fine energy group within a multi group was 17 in the present calculation condition, 16 (minimum number – 1) was used as the maximum number of orthogonal bases in the present study. The results showed that this number was enough to calculate effective cross sections and reaction rates.

III.A.2. Numerical Results and Discussions

At first, behavior of singular values and orthogonal bases was discussed in order to grasp an actual image of these quantities. In the following description, group 88 (6.16 eV – 7.52 eV) in the XMAS 172 energy structure was considered since a large resonance of U-238 exists in this group. Typical spectra obtained by ultra-fine group slowing-down calculation in homogeneous UO₂ geometry with various background cross sections were shown in Fig. 3. Singular values obtained by SVD of ultra-fine group spectra were plotted in Fig. 4. Note that singular values were normalized so that the largest singular value was 1.0. Figure 4 indicated that singular values are rapidly decreasing as the order increases. As described in Sec. II.C., singular values represent the contribution of corresponding expansion basis. Therefore, we can expect that the ultra-fine group spectra can be expressed by the small number of orthogonal basis. Next, typical orthogonal bases obtained by SVD were shown in Fig. 5. Orthogonal basis of the lower-order represented general trend of ultra-fine group spectra in Fig. 3 while that of the higher-order captured the more detailed structure of ultra-fine group spectra. Figure 6 showed ultra-fine group spectra of group 88 in UO₂ pellet (Fig. 2-(a), No.2). As the order of expansion in the RSE method increased, the present calculation result was rapidly approaching the reference, showing good convergence as expected.

Now let us move to the comparison of effective microscopic cross sections and reaction rates. Firstly, the relative differences of the effective microscopic total cross sections and microscopic total reaction rates in XMAS 172 energy group were calculated by $(RSE - UFG)/UFG$. Tables VI and VII showed the maximum absolute relative differences of effective microscopic total cross sections and total reaction rates for resonance nuclides in Fig. 2-(a) or (b) at the entire energy range (10^{-5} eV – 20 MeV). The number of bases was fixed to 16. As shown in Tables VI and VII, the differences were less than two percent for major resonance nuclides. Therefore, the RSE method accurately reproduced the reference reaction rates of resonance nuclides. This result also indicated that the orthogonal bases obtained by spectra in homogeneous geometries can well represent spectra in heterogeneous geometry.

Secondly, the impact of the number of bases used in the RSE method was discussed. Group 88 (6.16 eV – 7.52 eV) in the XMAS 172 group structure was also considered. In Figs. 7 and 8, the differences of the microscopic effective total cross sections were rapidly decreased as the expansion order increases and almost converged

by four orthogonal bases for Fig. 2-(a) and eight bases for Fig. 2-(b), respectively. This result indicated that the complicated ultra-fine group spectra in resonance energy range can be accurately represented by the limited number of orthogonal basis based on ROM, which is described in Sec. II.C. The similar trend (rapid reduction of error) was also observed in other energy groups. Though the number of bases was fixed for all groups in the present study, these can be independently set at each group. The adaptive choice of the number of bases will increase the calculation efficiency of the RSE method.

Finally, the capability to treat the resonance interference effect was discussed. The differences of the reference effective total cross sections for U-235, U-238, Pu-239, and Pu-240 in MOX fuel at Fig. 2-(b) and -(c) were shown in Fig. 9. The reference effective total cross section was obtained by UFG calculations using MOC. The difference was defined by $((c) - (b)) / (b)$. The energy range of Fig. 9 included major resolved resonance of U-235 and U-238 (1 eV – 10^5 eV). Figure 9 showed that the effective total cross sections of MOX fuel in (b) and (c) are different due to different material arrangement and the resonance interference effect. The differences of effective total cross sections and total reaction rates, which were obtained by the RSE method for Fig. 2-(b) and -(c), were shown in Figs. 10 and 11. The difference was also calculated by $(RSE - UFG)/UFG$. The difference was very small, and these results indicated that the RSE method can accurately treat the resonance interference effect. Namely, the neutron spectra in the heterogeneous geometry, in which the resonance interference effects appeared, were accurately expressed by the linear combination of orthogonal basis obtained in the homogeneous geometry in the present study.

Before moving to the next benchmark problem, the convergence property of numerical calculation was described. As shown in Fig. 1, two parameters should be converged in the RSE method, *i.e.*, the flux moments (expansion coefficients) and the slowing down source. The numbers of inner iterations of a MOC calculation for Fig. 2-(a), -(b), or -(c) were approximately 30 and 10 for the fast and the thermal energy groups, respectively. On the other hand, the convergence of slowing down source within a multi-group was rather fast thus the convergence of flux moments in MOC dominated the total convergence of the RSE method.

III.B. Pin-cell Geometry with Annularly Subdivided Pellet

III.B.1. Calculation Conditions

A MOX pin-cell with annularly subdivided pellet was used to confirm the applicability of the RSE method for the spatial self-shielding effect with temperature distribution. Specification of pin-cell geometry was provided in Table I and the fuel pellet was annularly divided into ten equal volume regions. The composition of each material was shown in Table II. The two temperature distributions were considered: the radial and the flat distributions as shown in Table VIII [7].

The number of ultra-fine group spectra to generate the orthogonal bases (Step (1)-(2) in Sec. II.F.) was defined by the numbers of background cross sections for each material described in Sec. III.A.1. The background cross sections in Table V were used for each material and temperature, which means that 120 points in radial temperature distribution cases (11 points \times 10 temperature for fuel, 9 points \times 1 temperature for cladding, and 1 point for moderator) and 21 points in flat temperature distribution cases (11 points \times 1 temperature for fuel, 9 points \times 1 temperature for cladding, and 1 point for moderator). The number of the orthogonal bases used in the RSE method was fixed 16 as discussed in Sec. III.A.

III.B.2. Numerical Results and Discussions

The effective microscopic total cross sections and microscopic total reaction rates of U-238 and Pu-239 were compared since these nuclides were dominant resonance nuclides in the MOX pellet and the impact of these nuclides to neutronics characteristics was large. Relative differences of the effective microscopic total cross sections and total reaction rates between RSE and UFG were calculated. The differences in the radial and the flat temperature distributions were shown in Figs. 12 and 13, respectively. Figure 14 showed the difference of the effective cross section and reaction rate between RSE and UFG in group 88 along with the pellet radial direction. These figures showed that the differences are small and the RSE method can accurately treat the spatial self-shielding effect regardless of the temperature distribution.

The difference of U-238 effective total cross section and total reaction rate for the radial temperature distribution case (Fig. 12) was smaller than that for the flat temperature distribution case (Fig. 13). These results seemed to be inconsistent since the radial temperature distribution case utilized a more complicated calculation condition. These

results can be explained by the characteristics of the RSE method. The spectra to generate the orthogonal bases in Fig. 12 was more diverse than those in Fig. 13, since various temperature condition was considered in Fig. 12. To confirm this estimation, the reaction rate of U-238 was calculated in the flat temperature distribution case with the orthogonal bases generated from both the flat and the radial temperature distribution cases in Table VIII. Relative differences in the reaction rates between RSE and UFG were shown in Fig. 15. The differences of this case were smaller than those in the flat temperature distribution case with the orthogonal bases only from the flat temperature distribution in Table VIII (Fig. 13). The present results suggested the importance of the choice of input spectra used to construct an orthogonal basis. Namely, the utilization of various spectra was favorable from the calculation accuracy. Our supplemental sensitivity study on the choice of input ultra-fine group spectra indicated that consideration of three temperature points (highest, average, and lowest) was sufficient to generate an accurate orthogonal basis in the RSE method. This means that all temperatures that appeared in the calculation geometry are not necessary but the ultra-fine group spectra should span the variations in a calculation geometry.

III.C. Unit Assembly Geometry

III.C.1. Calculation Conditions

A 17×17 UO₂ fuel assembly based on the VERA benchmark problem [26] was used to confirm the applicability of the RSE method for larger geometries. The quarter symmetry was considered as shown in Fig. 16. Two material regions A and B in Fig. 16 were chosen to consider different self-shielding conditions. For simplicity, the following approximations were used: 1) 3.1 wt% UO₂ was composed of U-235, U-238, and O-16, 2) gap and cladding in a fuel rod were homogenized, 3) inter-assembly gap was not modeled, 4) boron was not included in the moderator. Specifications of the geometry and nuclide number densities are shown in Table IX and Table X, respectively. The temperature of all material was 600 K. the reflective boundary condition was assumed for all boundaries.

As the multi-cell cases (Sec. III.A), the number of ultra-fine group spectra to generate the orthogonal bases (Step (1)-(2) in Sec. II.F.) was 21, which came from the numbers of background cross sections for UO₂ (11 points), cladding (9 points) and H₂O

(1 point) as shown in Table V. The number of the orthogonal bases used in the RSE method was fixed to 16 as discussed in the previous two verifications.

Multi-group cross section of each material region for eigenvalue calculation was prepared using the effective cross sections obtained by RSE and UFG calculation in the assembly as follows: 1) the effective cross sections (capture, production, elastic scattering, and total) obtained by RSE or UFG were used in the major resonance energy range (from group 34 to group 124 in XMAS 172 group: ~ 1 eV - $\sim 10^5$ eV) for UO₂ and cladding, 2) infinite dilution cross section was used for moderator, and fast ($>10^5$ eV) or thermal (<1 eV) energy range for cladding. It should be noted that other multi-group cross sections including fission spectrum are generated by FRENDDY/MG [27]. The same multi-group cross sections are used throughout the eigenvalue calculations except for the effective cross section in the major resonance range in order to focus on the impact of resonance calculations on the results such as eigenvalue or pin-power. Multi-group eigenvalue calculation was performed using the MOC transport solver GENESIS [23]. The calculation condition of MOC for eigenvalue calculation was shown in Table XI.

III.C.2. Numerical Results and Discussions

Relative differences in the effective total cross sections and total reaction rates between RSE and UFG were calculated. The results for U-235 and U-238 at regions A and B of Fig. 16 in the major resonance energy range were shown in Figs. 17 and 18, respectively. The differences were small in two regions.

Accuracy of flux and source are compared to consider the characteristics of the RSE method. Ultra-fine group spectra and sources in regions A and B of Fig. 16 in the major resonance energy range are shown in Figs. 19 and 20, respectively. They show reasonable agreement with the reference results. The ultra-fine group spectrum shows local deviation from the reference result since the difference is shown by the relative value and spectrum shows a very small value at some energy points. However, reaction rates or effective cross sections are obtained with sufficient accuracy by the RSE method since these parameters are integrated values. The difference of source was relatively small because the source in the RSE method was obtained by the slowing down equation in the present study as described in Sec. II.D.

The current computation time of the RSE method is approximately 140 minutes and that of the UFG calculation is approximately 370 minutes for a single assembly

calculation in the present study. However, it should be noted that the numerical algorithms of the RSE method were not yet optimized since the purpose of the present study was a demonstration of the principle of the present method. Calculation time can be further reduced by optimization of energy group structure, discretization parameters for MOC, and improvements of numerical algorithms. Our preliminary study so far suggests that computation time can be reduced by approximately factor 20 considering these improvements. The number of inner iterations of MOC was between 5 to 20 at each energy group in the RSE calculation for the assembly (Fig. 16). Since MOC calculation for flux moments in the RSE method is quite similar to the conventional one, the coarse mesh fine difference (CMFD) acceleration method [28] could be applied to the RSE method. This is also one of the future tasks to reduce computation time.

Eigenvalue and pin-power distribution were compared in Table XII. The difference was calculated by $|(RSE - UFG)/UFG|$. Table XII showed that discrepancies of these neutronics characteristics were small. This result suggests that the differences of the effective cross section, reaction rate, and flux shown in Fig. 17 to Fig. 20 have small impacts to eigenvalue and pin-power distribution. Note that since boron was not included in moderator for simplicity, eigenvalues in Table XII were estimated to be larger than the value described in the VERA benchmark problem (k -effective = 1.183360 ± 0.000024) [26].

IV. CONCLUSIONS

The Resonance calculation based on energy Spectrum Expansion (RSE) method is newly proposed in this paper. In the RSE method, ultra-fine group neutron spectra in heterogeneous geometry are expanded by an orthogonal basis on energy. The orthogonal basis is constructed with ultra-fine group neutron spectra obtained in homogeneous geometry through the singular value decomposition (SVD) and the low-rank-approximation (LRA). The neutron transport equation for expansion coefficients of angular flux is derived and is numerically solved by MOC.

This method applied to a 2×2 multi-cell geometries and a pin-cell with annularly subdivided fuel pellet with different fuel types, *i.e.*, UO_2 and MOX, to consider the resonance interference effect. In the pin-cell with subdivided pellet, the radial and the flat temperature distributions were used to consider the spatially dependent self-shielding effect with temperature distribution. The reaction rate or effective microscopic cross

section obtained by the RSE method were compared with the reference results by the ultra-fine group (UFG) heterogeneous calculation using MOC. These numerical results show the validity of this method which accurately reproduces the reference results obtained from the UFG calculation by MOC considering the resonance interference effect among different regions and the spatial self-shielding effect. As a more complicated and practical problem, eigenvalue calculations in UO₂ single fuel assembly have been carried out using the effective cross sections obtained by the UFG and RSE methods. Calculation results indicate that differences in eigenvalue and pin-power are sufficiently small. Therefore, UFG and RSE methods provide comparable results as a resonance calculation method in the present calculation conditions.

This study shows the feasibility of the present method. For practical applications, however, there are several issues to be addressed, especially from the viewpoint of computational efficiency. An efficient generation method of an orthogonal basis is desirable since the number of orthogonal bases is directly proportional to the computational cost. The validity of orthogonal bases considering various material compositions, *e.g.* depleted fuels, should be also confirmed. In the results of Sec. III.A, the same orthogonal basis is used to UO₂ and MOX fuels. Since the characteristics of MOX fuel is similar to that of depleted UO₂ fuels, the present result is evidence to show the applicability of the RSE method to such conditions. However, more extensive verifications considering actual lattice physics calculation conditions are desirable. The optimal choice of energy group to generate effective cross sections would be another issue. Finally, as a future task, this method will be applied to more complicated conditions/larger geometry, *e.g.*, multi-fuel assemblies, or full core geometry.

References

1. R. J. J. STAMM'LER and M. J. ABBATE, *Methods of steady-state reactor physics in nuclear design*, Academic Press, London (1983).
2. P. H. KIER and A. A. ROBBA, "RABBLE, A Program for Computation of Resonance Absorption in Multiregion Reactor Cells," ANL-7326, Argonne National Laboratory, 1967; <https://doi.org/10.2172/4245065>.
3. M. N. NIKOLAEV et al, "The Method of Subgroups for Considering the Resonance Structure of the Cross Sections in Neutron Calculations (Part 1)," *Sov. At. Energy.*, **29**, 1, 689 (1970); <https://doi.org/10.1007/BF01338769>.
4. D. G. CACUCI Ed., *Handbook of Nuclear Engineering*, Vol. 2, Chap.9, Springer, New York (2010).
5. M. L. WILLIAMS, "Correction of Multigroup Cross Sections for Resolved Resonance Interference in Mixed Absorbers," *Nucl. Sci. Eng.*, **83**, 1, 37 (1983); <https://doi.org/10.13182/NSE83-2>.
6. A. HÉBERT, "A Mutual Resonance Shielding Model Consistent with Ribon Subgroup Equations," *Proc. PHYSOR2014*, Chicago, IL, April 25-29, 2014 (2014).
7. H. MATSUMOTO, M. OUISLOUMEN, and T. TAKEDA, "Spatially Dependent Self-Shielding Method with Temperature Distribution for the Two-Dimensional Transport Code PARAGON" *J Nucl Sci Technol.*, **43**, 11, 133 (2006); <https://doi.org/10.1080/18811248.2006.9711225>.
8. F. RAHNEMA, S. DOUGLASS, and B. FORGET, "Generalized Energy Condensation Theory," *Nucl. Sci. Eng.*, **160**, 1, 41 (2008); <https://doi.org/10.13182/NSE160-41>.
9. L. ZHU and B. FORGET, "A Discrete Generalized Multigroup Energy Expansion Theory," *Nucl. Sci. Eng.*, **166**, 3, 239 (2010); <https://doi.org/10.13182/NSE09-84>.
10. R. LE TELLIER, D. FOURNIER, and J. RUGGIERI, "A Wavelet-based Finite Element Method for the Self-shielding Issue in Neutron Transport," *Nucl. Sci. Eng.*, **163**, 1, 34 (2009); <https://doi.org/10.13182/NSE163-34>.
11. W. YANG, H. WU, and Y. ZHENG, "Application of Wavelets Scaling Function Expansion Method in Resonance Self-shielding Calculation," *Ann. Nucl. Energy*, **37**, 5, 653 (2010); <https://doi.org/10.1016/j.anucene.2010.02.008>.
12. W. ROOIJEN, "Feasibility of Wavelet Expansion Method to Treat the Energy Variable," *Proc. PHYSOR2012*, Knoxville, TN, April 15-20, 2012 (2012).

13. C. C. STOKER and Z. J. WEISS, "Spatially Dependent Resonance Cross Sections in a Fuel Rod," *Ann. Nucl. Energy*, **23**, 9, 765 (1996); [https://doi.org/10.1016/0306-4549\(95\)00074-7](https://doi.org/10.1016/0306-4549(95)00074-7).
14. H. MATSUMOTO, M. OUISLOUMEN, and T. TAKEDA, "Development of Spatially Dependent Resonance Shielding Method," *J. Nucl. Sci. Tech.*, **42**, 8, 688 (2005); <https://doi.org/10.1080/18811248.2004.9726438>.
15. K. KIM, "Comparison between Spatially Dependent Embedded Self-Shielding and Subgroup Methods," *Trans. Am. Nucl. Soc.*, **119**, 1193 (2018).
16. H. S. ABDEL-KHALIK, "Feasibility Study of an Integrated Framework for Characterization of Uncertainties with Application to CANDU Steady State and Transient Reactor Physics Simulation," Canadian Nuclear Safety Commission (Jun. 2015).
17. A. YANKOV, "*Analysis of Reactor Simulation Using Surrogate Model*," Ph.D. Thesis, University of Michigan (2015).
18. M. MATSUSHITA, A. YAMAMOTO, and T. ENDO, "Development of a Reduced Order Model for Severe Accident Analysis Codes by Singular Value Decomposition Aiming Probabilistic Safety Margin Analysis," *J. Nucl. Sci. Technol.*, **57**, 5, 573 (2020); <https://doi.org/10.1080/00223131.2019.1699190>.
19. N. SUGIMURA and A. YAMAMOTO, "Resonance Treatment Based on Ultra-fine-group Spectrum calculation in the AEGIS Code," *J. Nucl. Sci. Technol.*, **44**, 7, 958 (2007); <https://doi.org/10.1080/18811248.2007.9711335>.
20. EIGEN; http://eigen.tuxfamily.org/index.php?title=Main_Page (accessed, 2017).
21. K. TADA et. al., "Development and Verification of a New Nuclear Data Processing System FRENDY," *J. Nucl. Sci. Technol.*, **54**, 7, 806 (2017); <https://doi.org/10.1080/00223131.2017.1309306>.
22. K. SHIBATA et al., "JENDL-4.0: A New Library for Nuclear Science and Engineering," *J. Nucl. Sci. Eng.*, **48**, 1, 1 (2011); <https://doi.org/10.1080/18811248.2011.9711675>.
23. A. YAMAMOTO, A. GIHO, Y. KATO, and T. ENDO, "GENESIS – A Three-dimensional Heterogeneous Transport Solver based on the Legendre Polynomial Expansion of Angular Flux Method," *Nucl. Sci. Eng.*, **186**, 1, 1 (2017); <https://doi.org/10.1080/00295639.2016.1273002>.

24. A. YAMAMOTO et al., “Derivation of Optimum Polar Angle Quadrature Set for the Method of Characteristics Based on Approximation Error of the Bickley Function,” *J. Nucl. Sci. Technol.*, **44**, 2, 129 (2007); <https://doi.org/10.1080/18811248.2007.9711266>.
25. H. KOIKE et al, “Integration of Equivalence Theory and Ultra-fine-group Slowing-down Calculation for Resonance Self-shielding Treatment in Lattice Physics Code GALAXY,” *J Nucl Sci Technol.*, **53**, 6, 842 (2016); <https://doi.org/10.1080/00223131.2015.1076745>.
26. A. T. CODFREY., “VERA Core Physics Benchmark Progression Problem Specifications,” CASL-U-2021-0131-004, Oak Ridge National Laboratory, 2014.
27. A. YAMAMOTO, T. ENDO, K. TADA, "Development of FRENDY Nuclear Data Processing Code: Generation Capability of Multi-group Cross Sections from ACE File," *Trans. Am. Nucl. Soc.*, **122**, 714 (2020).
28. K. S. SMITH, “Nodal Method Storage Reduction by Non-Linear Iteration,” *Trans. Am. Nucl. Soc.*, **44**, 265 (1984).

List of Tables

Table I. Dimensions of pin-cell (unit: cm)

Table II. Compositions of materials

Table III. Calculation conditions for MOC

Table IV. Energy group structure for ultra-fine group calculation

Table V. Background cross sections for ultra-fine group calculation in homogeneous geometry

Table VI. The maximum relative differences of microscopic effective total cross sections and total reaction rates calculated by the RSE method in Fig. 2-(a)

Table VII. The maximum relative differences of microscopic effective total cross sections and total reaction rates calculated by the RSE method in Fig. 2-(b)

Table VIII. Temperature distributions in the pin-cell geometries

Table IX. Dimensions of the assembly (unit: cm)

Table X. Compositions of material in the assembly

Table XI. Calculation conditions of MOC for assembly geometry

Table XII. Differences in eigenvalue and pin-power distribution of eigenvalue calculation for Fig. 16

List of Figures

Fig. 1. Flowchart of the RSE method

Fig. 2. Multi-cell geometries

Fig. 3. Spectra in homogeneous UO_2 obtained by ultra-fine group slowing down calculation for various background cross sections in group 88 (6.16 eV - 7.52 eV)

Fig. 4. Singular values for ultra-fine group spectra for group 88

Fig. 5. The orthogonal basis extracted from spectra in homogeneous geometries

Fig. 6. Reference and reconstructed ultra-fine group spectra in UO_2 (Fig. 2-(a), cell 2) for group 88 (6.16 eV - 7.52 eV). The legend shows the order of expansion

Fig. 7. Difference of effective total cross section in group 88 for various number of orthogonal bases in Fig. 2-(a)

Fig. 8. Difference of effective total cross section in group 88 for various number of orthogonal bases in Fig. 2-(b)

- Fig. 9. Difference of effective total cross sections in MOX fuel between Fig. 2-(b) and Fig. 2-(c) obtained by UFG with MOC
- Fig. 10. Differences of effective total cross sections and total reaction rates obtained by the reference UFG and RSE (U-235, U-238, Pu-239, and Pu-240 in MOX fuel, Fig. 2-(b))
- Fig. 11. Differences of effective total cross sections and total reaction rates obtained by the reference UFG and RSE (U-235, U-238, Pu-239, and Pu-240 in MOX fuel, Fig. 2-(c))
- Fig. 12. Differences of effective total cross sections and total reaction rates obtained by the reference UFG and RSE (U-238, Pu-239, using radial temperature distribution). The legend shows the subdivided pellet region shown in Table VIII
- Fig. 13. Differences of effective total cross sections and total reaction rates obtained by the reference UFG and RSE (U-238, Pu-239, using flat temperature distribution). The legend shows the subdivided pellet region shown in Table VIII
- Fig. 14. Differences of effective total cross sections and total reaction rates in a pellet obtained by the reference UFG and RSE (U-238 and Pu-239, group 88: 6.16 eV - 7.52 eV)
- Fig. 15. Differences of effective total cross sections and total reaction rates of U-238 obtained by the reference UFG and RSE in the flat temperature distribution case. The orthogonal bases are generated from both the flat and the radial temperature distribution in Table VIII. The legend shows the subdivided pellet region shown in Table VIII
- Fig. 16. A 17×17 fuel assembly based on VERA benchmark problems
- Fig. 17. Differences of effective total cross sections and total reaction rates obtained by the reference UFG and RSE at region A in Fig. 16
- Fig. 18. Differences of effective total cross sections and total reaction rates obtained by the reference UFG and RSE at region B in Fig. 16
- Fig. 19. Differences of ultra-fine group spectra and source obtained by the reference UFG and RSE at region A in Fig. 16
- Fig. 20. Differences of ultra-fine group spectra and source obtained by the reference UFG and RSE at region B in Fig. 16

Table I

Dimensions of pin-cell (unit: cm)

Pellet radius	0.4095
Cladding outer radius	0.4750
Cell pitch	1.2600

Table II

Compositions of materials

Material	Nuclide	Number density [1/barn/cm]	Material	Nuclide	Number density [1/barn/cm]
Fuel (UO ₂)	¹⁶ O	4.68618E-02	Fuel (MOX)	¹⁶ O	4.59163E-02
	²³⁵ U	1.13836E-03		²³⁵ U	4.16028E-05
	²³⁸ U	2.22834E-02		²³⁸ U	2.04972E-02
Moderator (H ₂ O)	¹ H	4.41629E-02		²³⁸ Pu	4.87049E-05
	¹⁶ O	2.20897E-02		²³⁹ Pu	1.40652E-03
Cladding (Zirconium)	⁹⁰ Zr	1.96348E-02		²⁴⁰ Pu	5.55429E-04
	⁹¹ Zr	4.28188E-03		²⁴¹ Pu	2.40495E-04
	⁹² Zr	6.54495E-03		²⁴² Pu	1.19746E-04
	⁹⁴ Zr	6.63272E-03		²⁴¹ Am	4.80973E-05
	⁹⁶ Zr	1.06856E-03			

Table III

Calculation conditions for MOC

Ray trace width	0.05 cm	
Number of azimuthal angles	32 for 2 π	
Number of polar angles	6 for π (the TY quadrature set [24])	
Energy group structure	Multi group	XMAS 172 [4]
	Ultra-fine group	120,000 (Table IV)
Convergence criterion	Scalar flux (for UFG)	10 ⁻⁵
	Moment of flux: ϵ_j (for RSE)	10 ⁻⁵

Table IV

Energy group structure for ultra-fine group calculation

Upper energy boundary [eV]	Number of divisions (Equal division for lethargy)
20,000,000	10,000
52,475	56,000
9118.8	12,000
4307.4	12,000
961.12	8,000
130.07	12,000
0.32242	10,000
Lower energy boundary: 0.00001 eV	

Table V

Background cross sections for ultra-fine group calculation in homogeneous geometry

	Background cross section [barn]
Fuel (UO ₂ and MOX)	1.00e+10, 2.00e+04, 3.60e+03, 1.00e+03, 2.60e+02, 1.40e+02, 6.40e+01, 5.20e+01, 2.80e+01, 1.00e+01, 1.00E-03
Moderator (H ₂ O)	1.00e+10
Cladding (Zirconium)	5.00e+06, 5.00e+05, 1.00e+05, 5.00e+04, 1.00e+04, 5.00e+03, 1.00e+03, 5.00e+02, 5.00e+01

Table VI

The maximum relative differences of microscopic effective total cross sections and total reaction rates calculated by the RSE method in Fig. 2-(a)

Material	Nuclide	Effective total cross section		Total reaction rate	
		Maximum error [%]	Corresponding energy group	Maximum error [%]	Corresponding energy group
UO ₂ (in cell 1)	²³⁵ U	0.06	62	0.49	75
	²³⁸ U	0.17	64	0.25	66
UO ₂ (in cell 2)	²³⁵ U	0.07	62	0.54	75
	²³⁸ U	0.20	64	0.27	66
Cladding (in cell 1)	⁹⁰ Zr	0.69	49	0.68	49
	⁹¹ Zr	1.21	49	1.19	49
	⁹² Zr	0.71	51	0.63	51
	⁹⁴ Zr	0.06	43	0.39	47
	⁹⁶ Zr	2.85	63	2.74	63
Cladding (in cell 2)	⁹⁰ Zr	0.62	49	0.61	49
	⁹¹ Zr	1.12	49	1.11	49
	⁹² Zr	0.61	51	0.54	51
	⁹⁴ Zr	0.05	43	0.35	47
	⁹⁶ Zr	2.46	63	2.36	63

Table VII

The maximum relative differences of microscopic effective total cross sections and total reaction rates calculated by the RSE method in Fig. 2-(b)

Material	Nuclide	Effective total cross section		Total reaction rate	
		Maximum error [%]	Corresponding energy group	Maximum error [%]	Corresponding energy group
MOX	²³⁵ U	0.03	69	0.42	64
	²³⁸ U	0.63	64	0.39	69
	²³⁸ Pu	0.17	66	0.47	66
	²³⁹ Pu	0.13	63	0.41	64
	²⁴⁰ Pu	1.22	63	1.14	69
	²⁴¹ Pu	0.12	64	0.53	64
	²⁴² Pu	0.08	69	1.49	69
	²⁴¹ Am	0.62	69	0.52	69
UO ₂	²³⁵ U	0.04	62	0.44	64
	²³⁸ U	0.60	64	0.34	64
Cladding (in MOX cell)	⁹⁰ Zr	0.25	49	0.23	49
	⁹¹ Zr	0.88	49	0.86	49
	⁹² Zr	0.65	49	0.63	49
	⁹⁴ Zr	0.05	47	0.31	47
	⁹⁶ Zr	1.49	63	1.42	63
Cladding (in UO ₂ cell)	⁹⁰ Zr	0.29	49	0.26	49
	⁹¹ Zr	0.92	49	0.89	49
	⁹² Zr	0.67	49	0.65	49
	⁹⁴ Zr	0.05	47	0.32	47
	⁹⁶ Zr	1.65	63	1.57	63

Table VIII

Temperature distributions in the pin-cell geometries

Region		Temperature [K]	
		Flat distribution	Radial distribution
Fuel	01 (inner)	997 for each region	1190
	02		1140
	03		1100
	04		1060
	05		1010
	06		970
	07		930
	08		890
	09		860
	10 (outer)		820
Cladding		600	
Moderator			

Table IX

Dimensions of the assembly (unit: cm)

Pellet radius	0.4096
Cladding outer radius	0.4750
Cell pitch	1.2600
Inner Guide Tube Radius	0.5610
Outer Guide Tube Radius	0.6020
Inner Instrument Tube Radius	0.5590
Outer Instrument Tube Radius	0.6050

Table X

Compositions of material in the assembly

Material	Nuclide	Number density [1/barn/cm]
Fuel (UO ₂)	¹⁶ O	4.57640E-02
	²³⁵ U	7.18132E-04
	²³⁸ U	2.21639E-02
Moderator (H ₂ O)	¹ H	4.42033E-02
	¹⁶ O	2.21017E-02
Cladding, instrument tube, or guide tube (Zirconium)	⁹⁰ Zr	1.96035E-02
	⁹¹ Zr	4.27506E-03
	⁹² Zr	6.53451E-03
	⁹⁴ Zr	6.62215E-03
	⁹⁶ Zr	1.06686E-03

Table XI

Calculation conditions of MOC calculation for assembly geometry

Ray trace width	0.05 cm	
Number of azimuthal angles	32 for 2π	
Number of polar angles	4 for π (the Gauss-Legendre quadrature set)	
Energy group structure	XMAS 172 [4]	
Convergence criterion	Scalar flux	1×10^{-5}
	k -effective	5×10^{-6}
Boundary condition	Reflective	

Table XII

Differences in eigenvalue and pin-power distribution of eigenvalue calculation for Fig. 16

k -effective		Difference of k -effective [%] $ (RSE - UFG)/UFG $	Difference of pin-power [%] $ (RSE - UFG)/UFG $	
RSE	UFG		MAX	RMS
1.33891	1.33932	3.1×10^{-2}	1.6×10^{-3}	7.2×10^{-4}

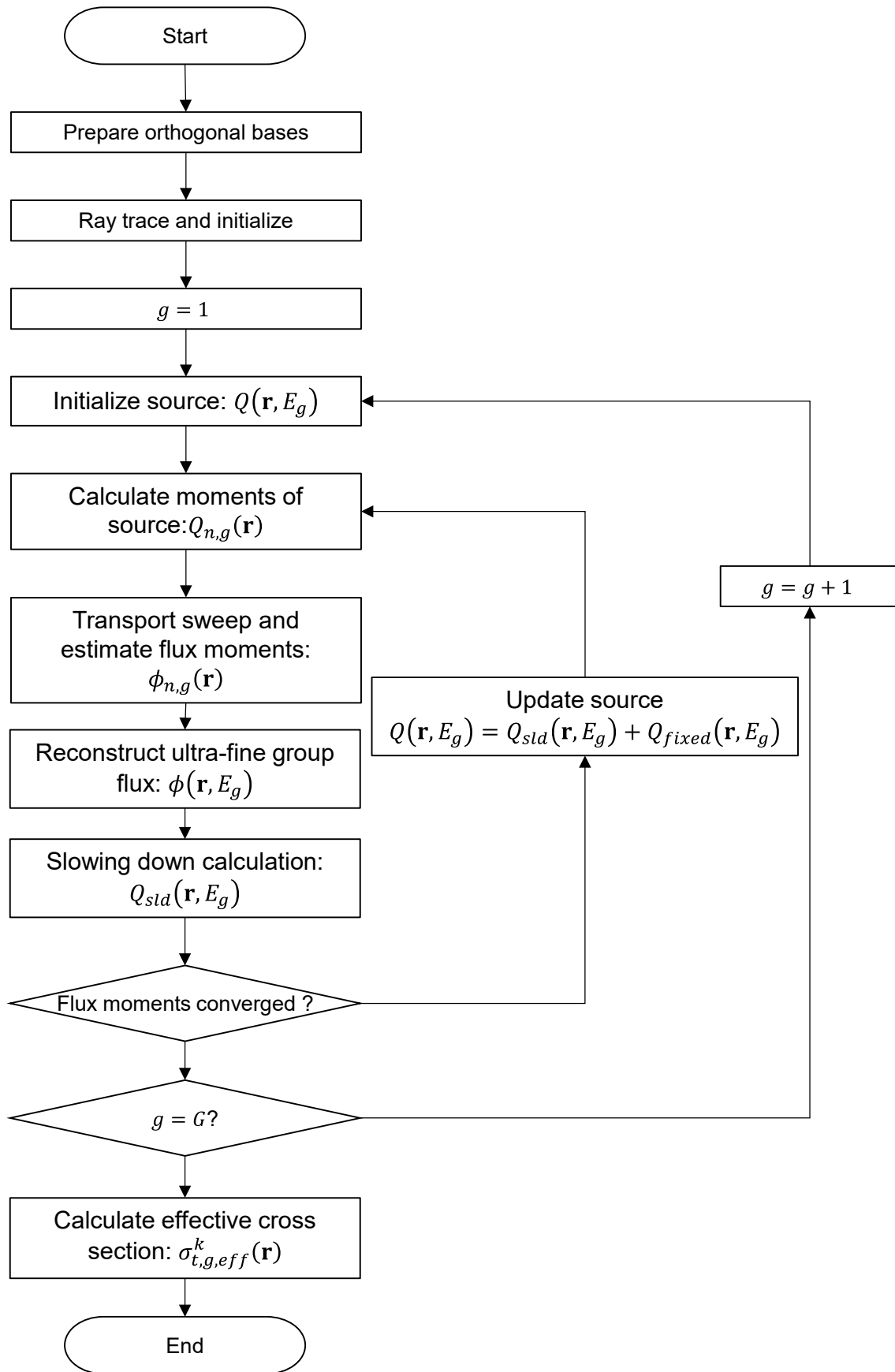


Fig. 1. Flowchart of the RSE method.

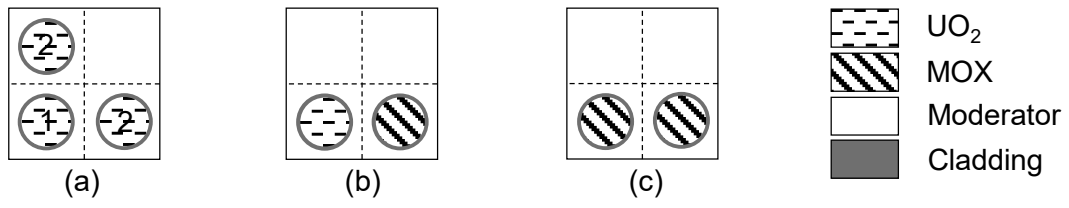


Fig. 2. Multi-cell geometries.

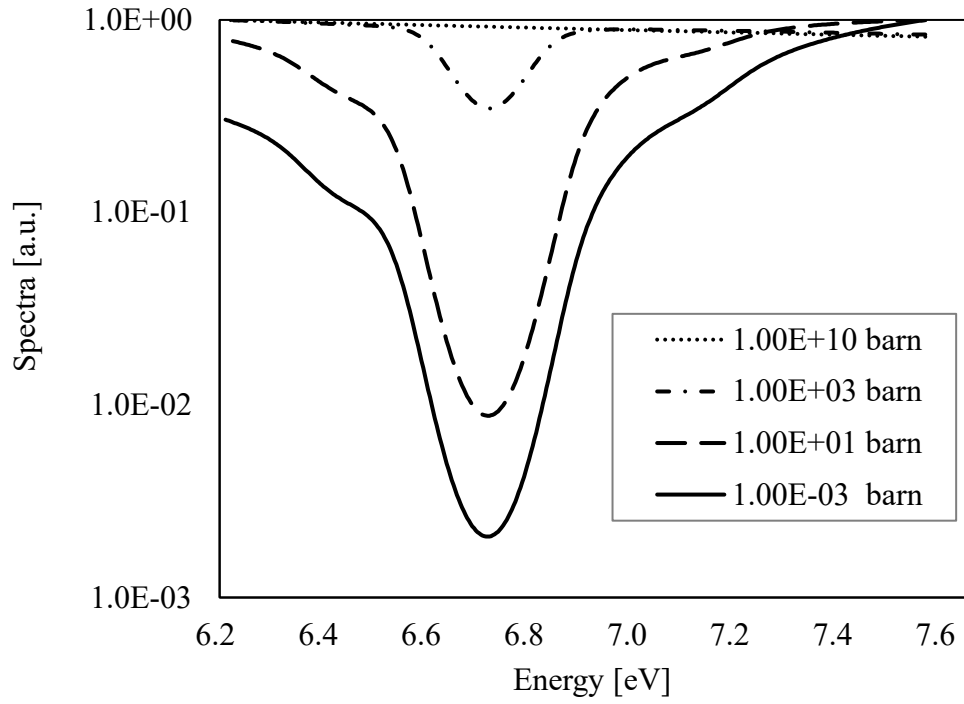


Fig. 3. Spectra in homogeneous UO₂ obtained by ultra-fine group slowing down calculation for various background cross sections in group 88 (6.16 eV - 7.52 eV).

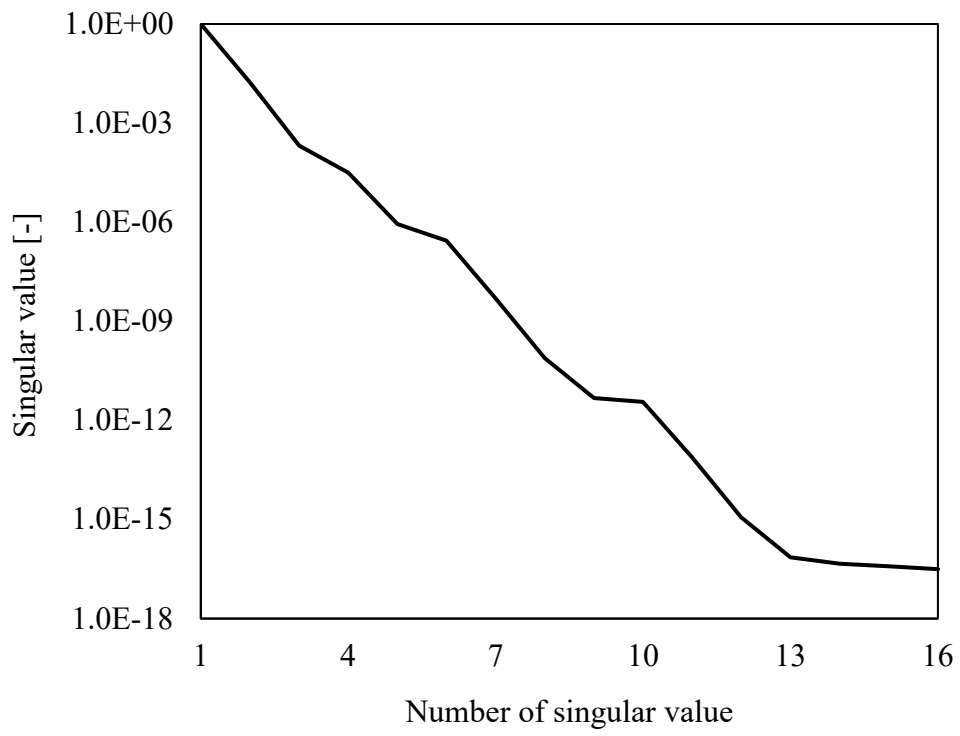


Fig. 4. Singular values for ultra-fine group spectra for group 88.

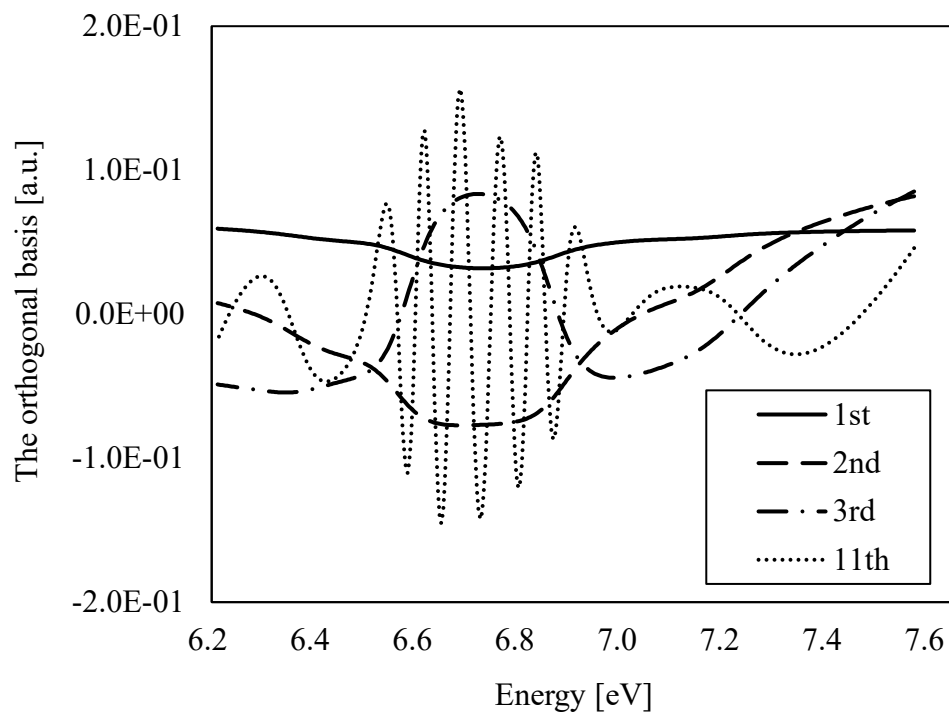


Fig. 5. The orthogonal basis extracted from spectra in homogeneous geometries.

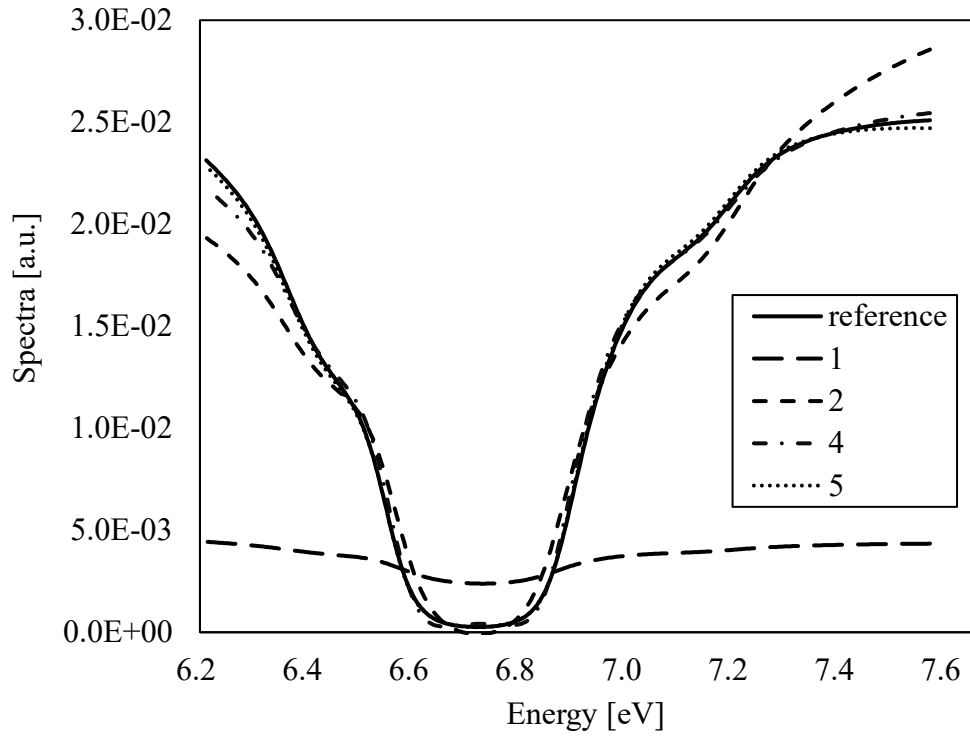


Fig. 6. Reference and reconstructed ultra-fine group spectra in UO₂ (Fig. 2-(a), cell 2) for group 88 (6.16 eV - 7.52 eV). The legend shows the order of expansion.

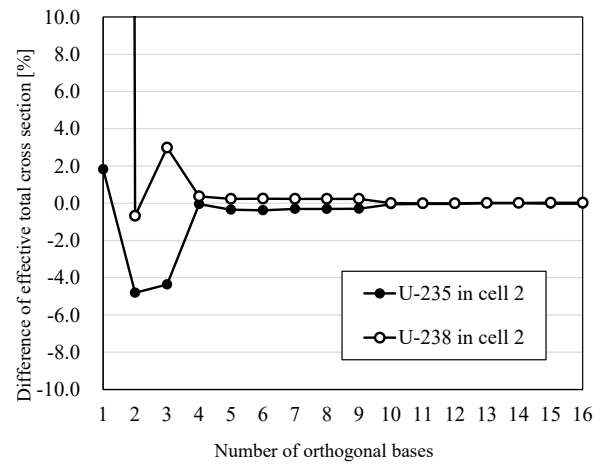
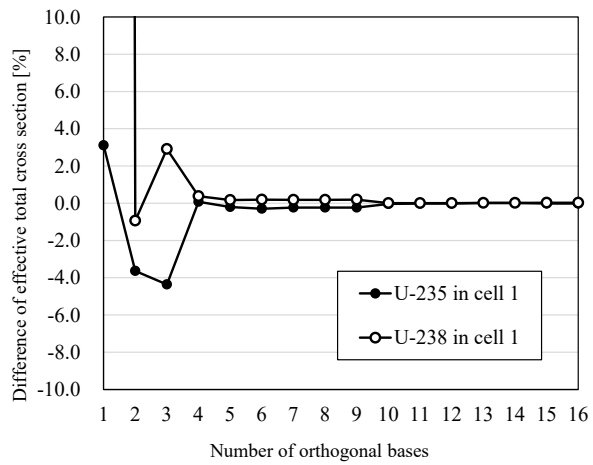


Fig. 7. Difference of effective total cross section in group 88 for various number of orthogonal bases in Fig. 2-(a).

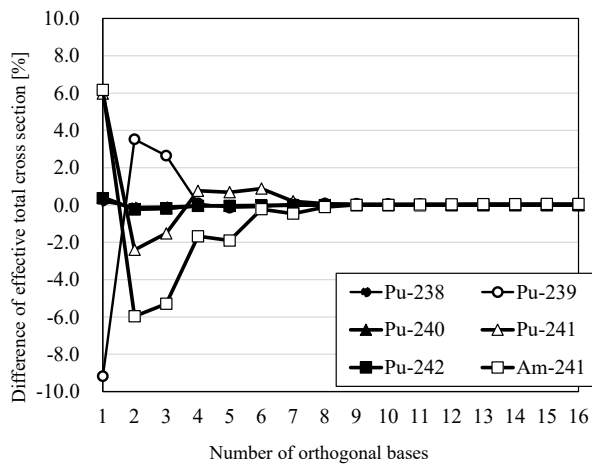
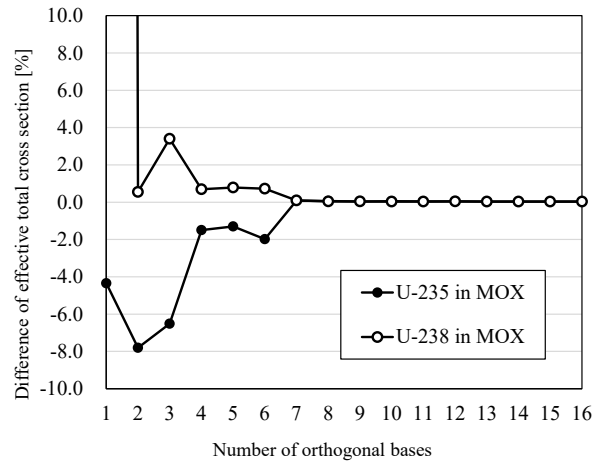
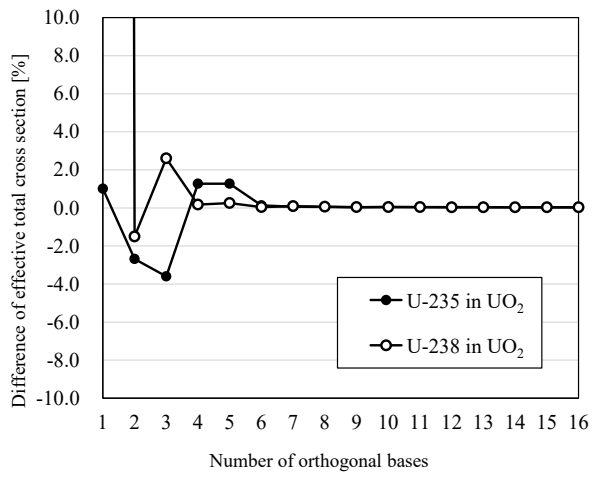
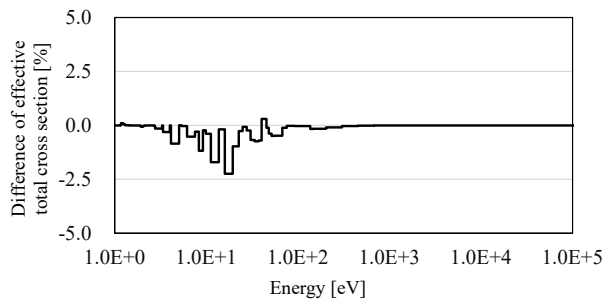
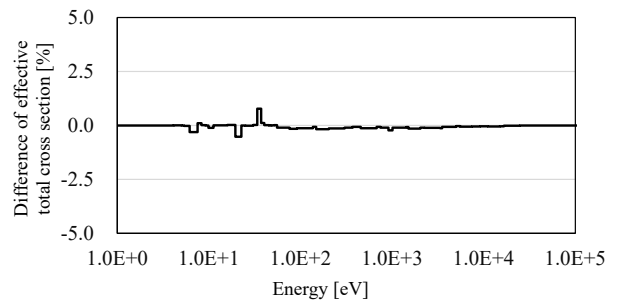


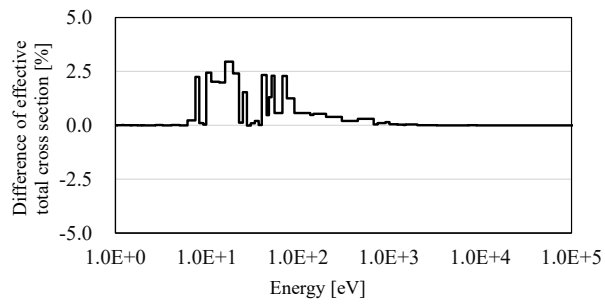
Fig. 8. Difference of effective total cross section in group 88 for various number of orthogonal bases in Fig. 2-(b).



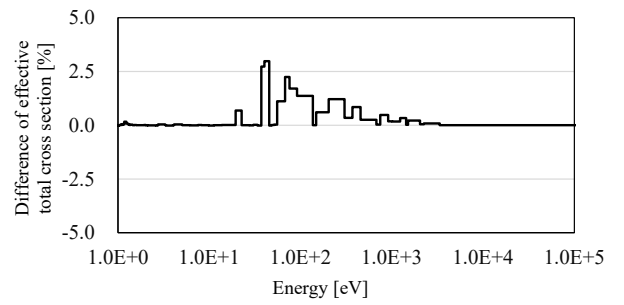
U-235



U-238



Pu-239



Pu-240

Fig. 9. Difference of effective total cross sections in MOX fuel between Fig. 2-(b) and Fig. 2-(c) obtained by UFG with MOC.

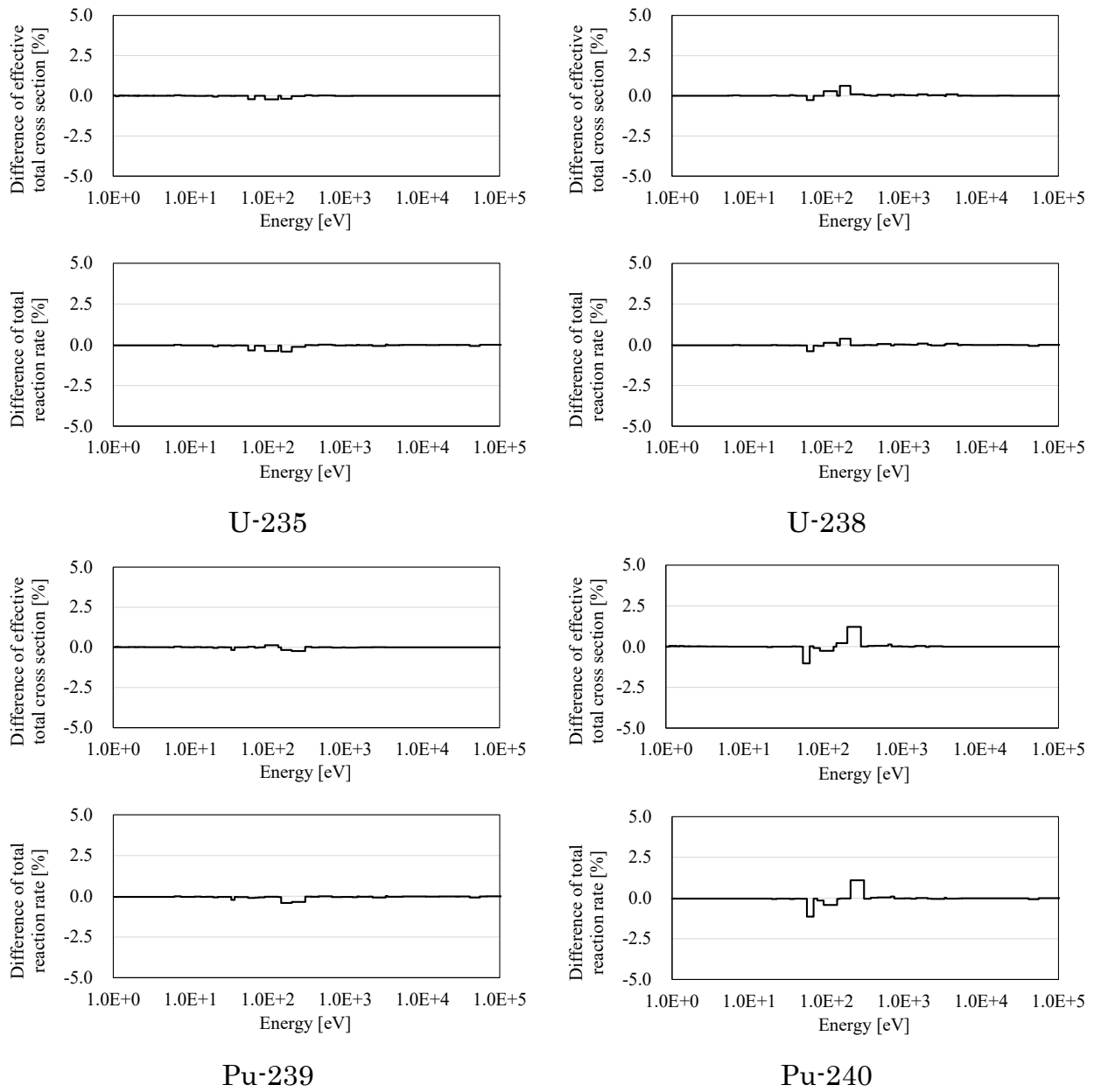


Fig. 10. Differences of effective total cross sections and total reaction rates obtained by the reference UFG and RSE (U-235, U-238, Pu-239, and Pu-240 in MOX fuel, Fig. 2-(b)).

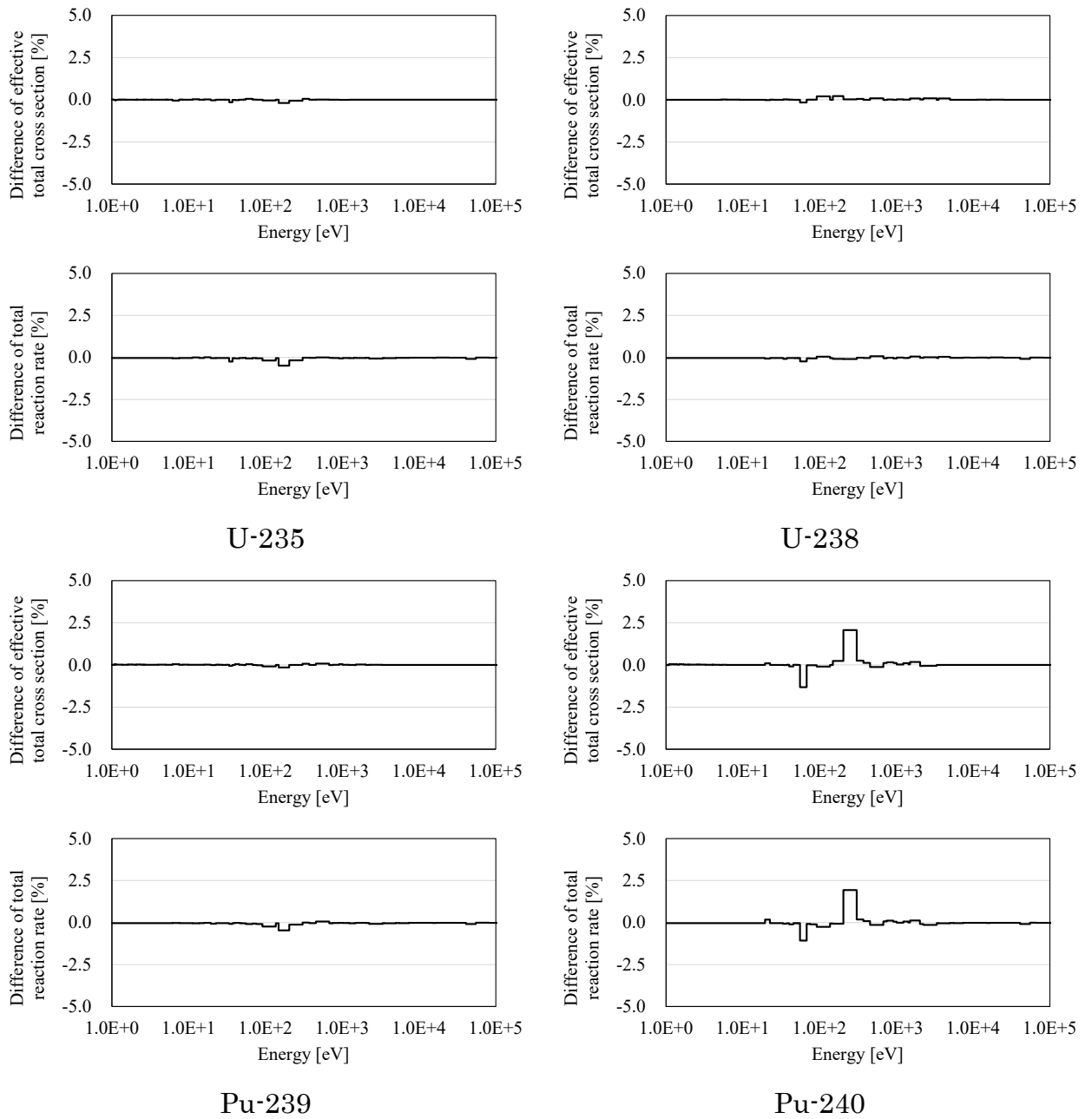


Fig. 11. Differences of effective total cross sections and total reaction rates obtained by the reference UFG and RSE (U-235, U-238, Pu-239, and Pu-240 in MOX fuel, Fig. 2-(c)).

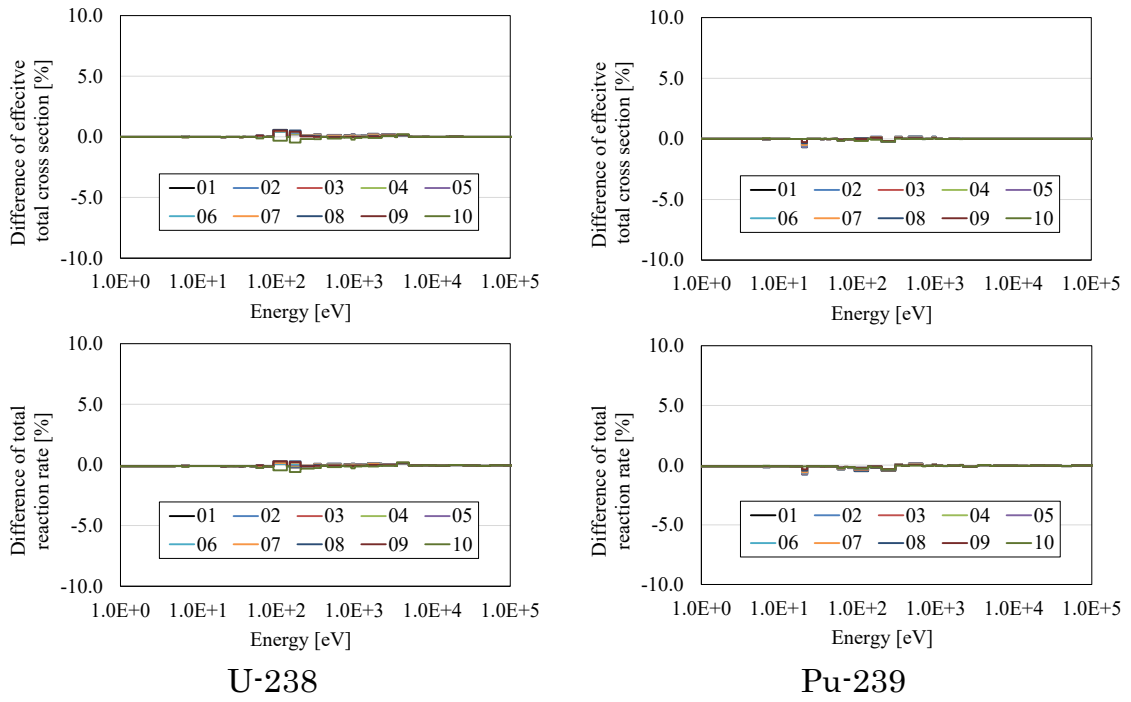


Fig. 12. Differences of effective total cross sections and total reaction rates obtained by the reference UFG and RSE (U-238, Pu-239, using radial temperature distribution). The legend shows the subdivided pellet region shown in Table VIII.

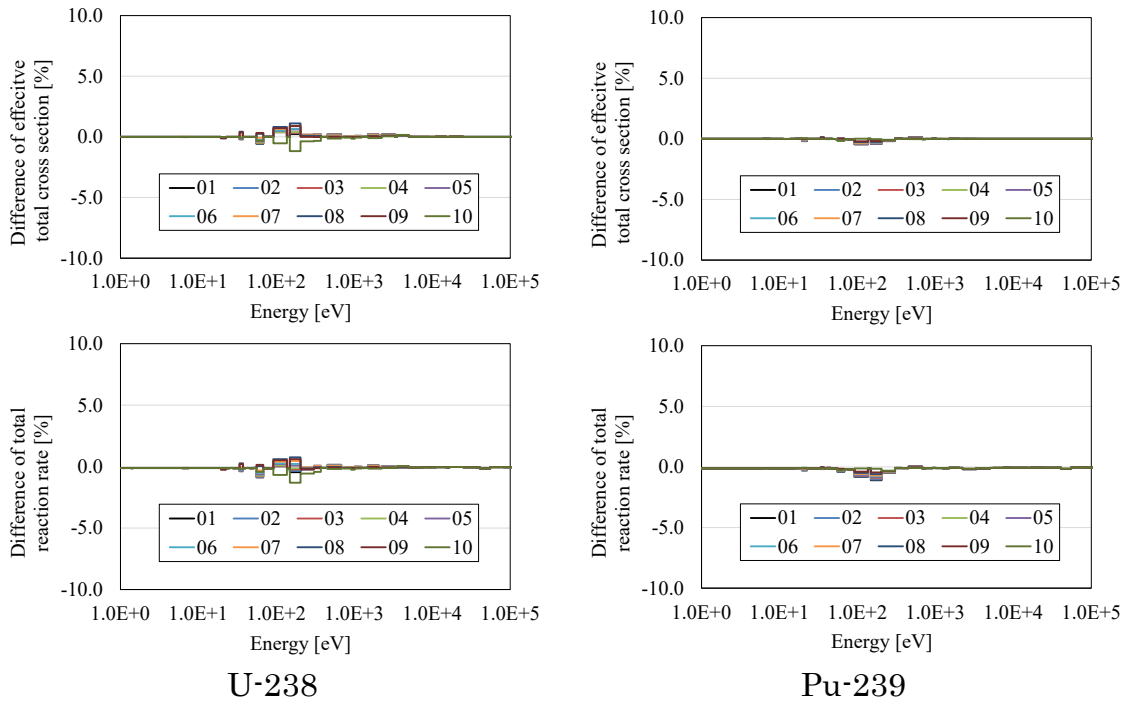


Fig. 13. Differences of effective total cross sections and total reaction rates obtained by the reference UFG and RSE (U-238, Pu-239, using flat temperature distribution). The legend shows the subdivided pellet region shown in Table VIII.

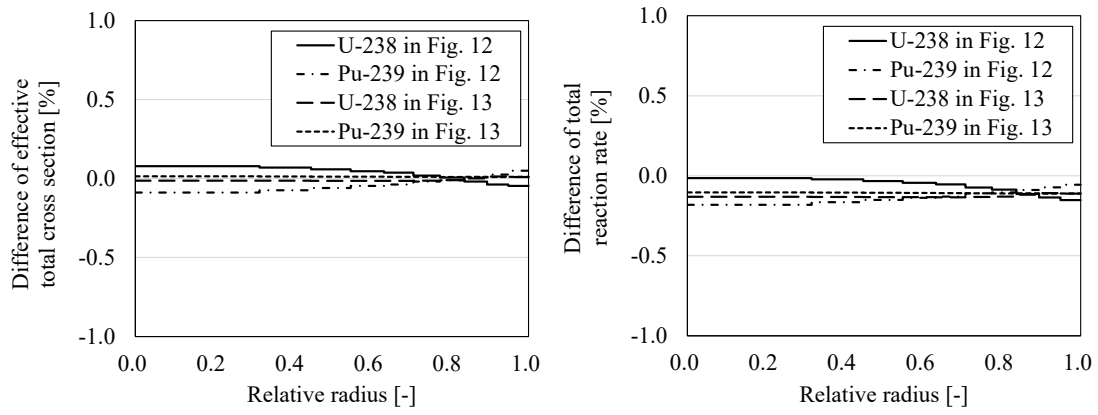


Fig. 14. Differences of effective total cross sections and total reaction rates in a pellet obtained by the reference UFG and RSE (U-238 and Pu-239, group 88: 6.16 eV - 7.52 eV).

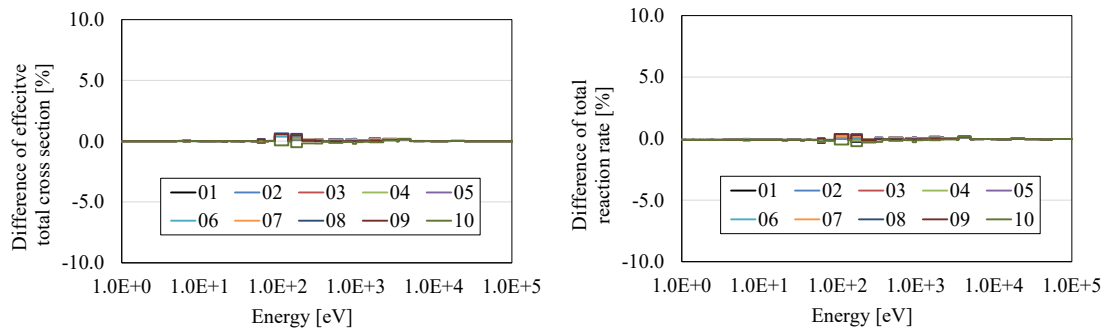


Fig. 15. Differences of effective total cross sections and total reaction rates of U-238 obtained by the reference UFG and RSE in the flat temperature distribution case. The orthogonal bases are generated from both the flat and the radial temperature distribution in Table VIII. The legend shows the subdivided pellet region shown in Table VIII.

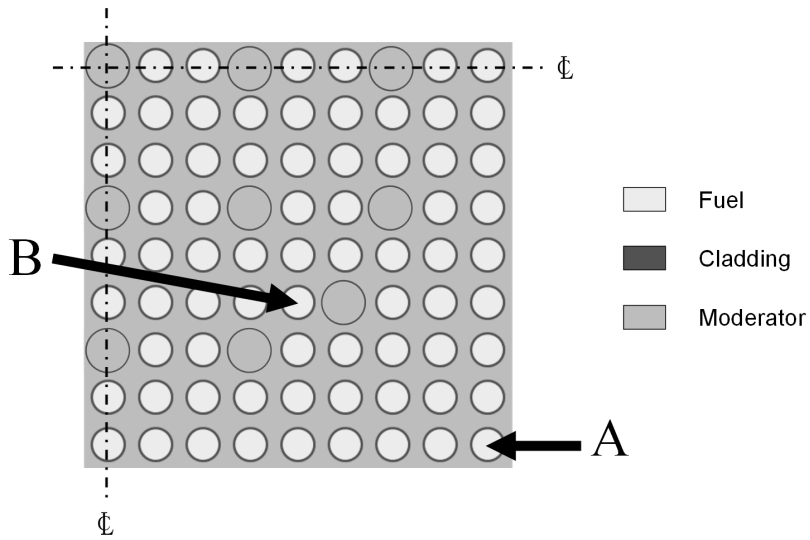


Fig. 16. A 17×17 fuel assembly based on VERA benchmark problems.

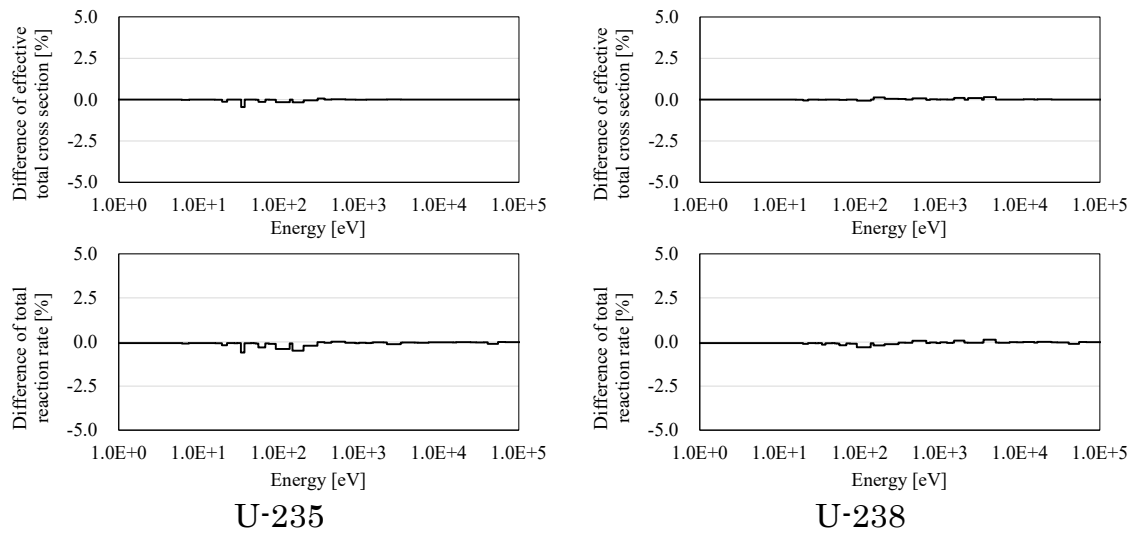


Fig. 17. Differences of effective total cross sections and total reaction rates obtained by the reference UFG and RSE at region A in Fig. 16.

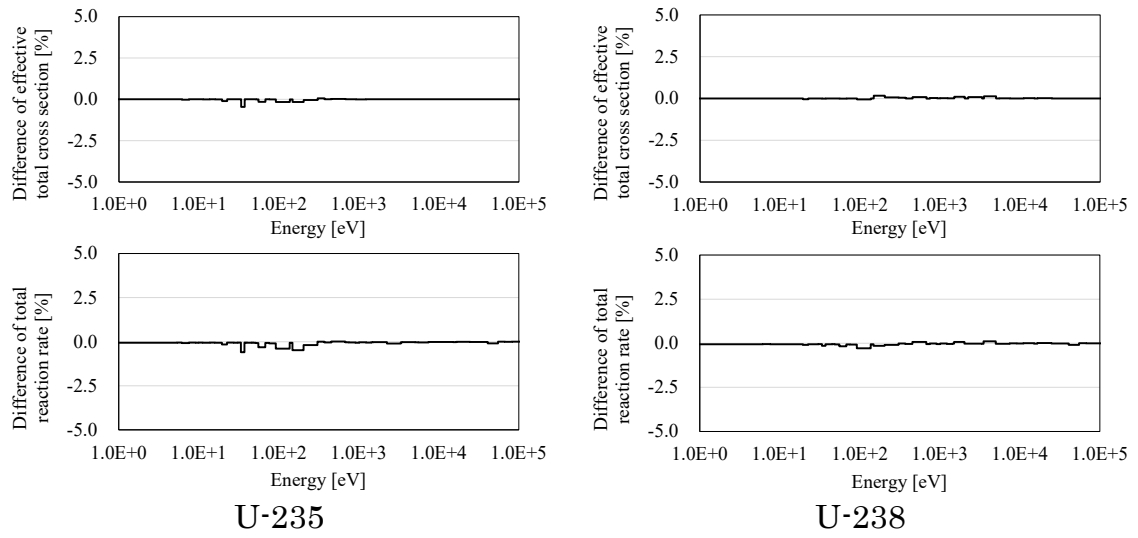


Fig. 18. Differences of effective total cross sections and total reaction rates obtained by the reference UFG and RSE at region B in Fig. 16.

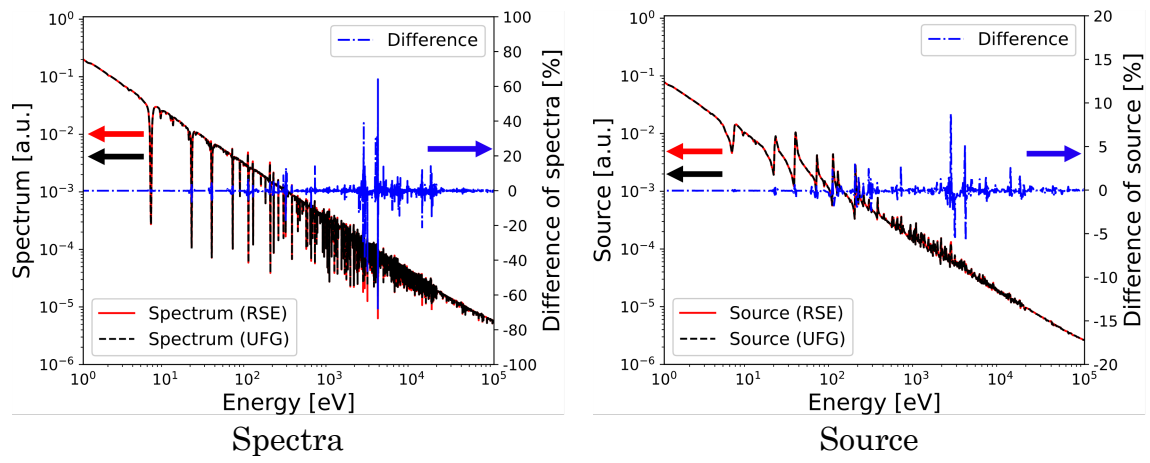


Fig. 19. Differences of ultra-fine group spectra and source obtained by the reference UFG and RSE at region A in Fig. 16.

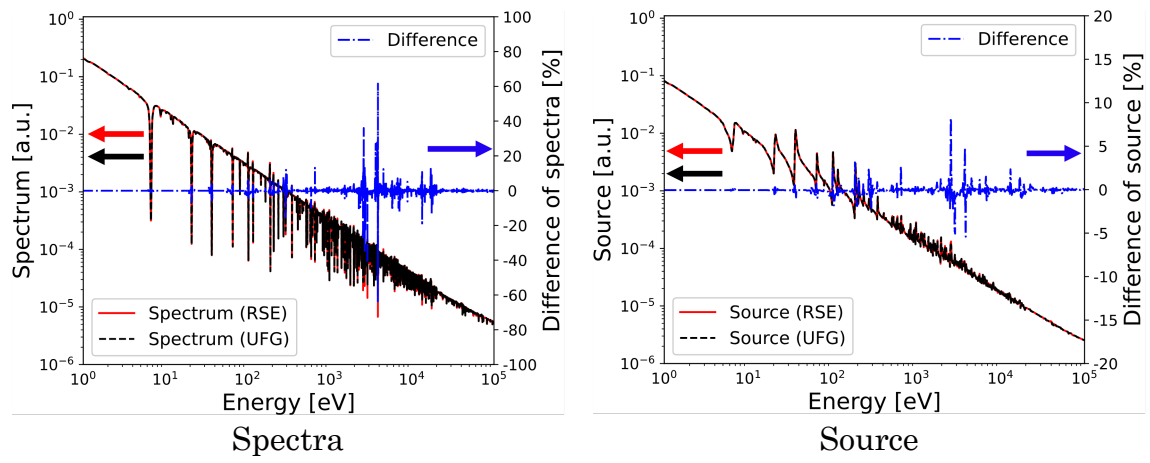


Fig. 20. Differences of ultra-fine group spectra and source obtained by the reference UFG and RSE at region B in Fig. 16.